5-2014

Theoretical Modeling of Laser-Induced Absorption Phenomena in Optical Materials

Chris Ferris
University of Nebraska-Lincoln, clferris@huskers.unl.edu

THEORETICAL MODELING OF LASER INDUCED ABSORPTION PHENOMENA IN OPTICAL MATERIALS

by

Chris Ferris

A THESIS

Presented to the Faculty of

The Graduate College at the University of Nebraska

In Partial Fulfilment of Requirements

For the Degree of Master of Science

Major: Electrical Engineering

Under the Supervision of Professor Natale Ianno

Lincoln, Nebraska

May, 2014

THEORETICAL MODELING OF LASER INDUCED ABSORPTION PHENOMENA IN OPTICAL MATERIALS

Chris Ferris, M. S.

University of Nebraska, 2014

Adviser: Natale J. Ianno

For over five decades, laser-induced damage and breakdown in optical materials has been an active field of research. As laser systems continually advance, new opportunities to study laser/material interactions arise. This thesis begins by presenting the damage mechanisms and absorption phenomena that lead to laser-induced breakdown. An in depth understanding of these processes led to the development of rate equations that describe electron density growth in a material exposed to a strong electromagnetic wave. These rate equations laid the foundation for the construction of a theoretical model. By using variable laser and material parameter inputs, the model calculates the laser-induced electron density in a material in order to predict damage occurrence. Simulations are compared with experimental results to determine the accuracy of the model. The results show great promise, but additional work must be done to increase confidence. Future developments of the model will lead to better accuracy and additional capabilities.

Acknowledgments

I would like to take this time to thank those who helped make this thesis a reality. Firstly, I would like to give my appreciation to my adviser Dr. Natale Ianno. From original discussions about whether pursuing graduate education was right for me, to sharing valuable advice on the world I am finally about to join, and of course all of the guidance and knowledge I received from him in between, I will always treasure my time spent under his leadership. A special thanks to Dr. Troy Anderson for his contributions, advice, and guidance in everything MATLAB, and for his willingness to explain techniques and share his knowledge in all areas of this project. He played a significant role in keeping the project moving forward. I would like to thank Nicholas Rowse for his assistance in the lab and for not only providing answers to all of my questions I had about the laser setup, but for working with me until I understood them. I also thank Sarkar Amitabha, Hrachya Kyureghian, Qinglei Ma, and Jinya Pu, my fellow graduate group members. They were always there to help me with any and everything they could. I was also privileged to spend time with them outside of a work mindset which helped keep me sane throughout my graduate career. Lastly I would like to thank Dr. Dennis Alexander and Dr. Ming Han for sitting on my graduate committee.

Contents

List of Figures

List of Tables

Chapter 1

Introduction

For several decades ultrafast ultra-intense lasers (UULs) have been used in a number of unique and exciting studies. The world's desire to push the limits of technology with these lasers have led to advancements in a variety of fields including homeland security, renewable energy, and advanced medical analysis.

The focus of this thesis stems from UULs applications in the area of transparent optical materials. Many military devices rely on optical systems for a variety of different purposes such as imaging systems, guidance systems, defense mechanisms, and much more. However, explaining the mechanisms of energy deposition from an UUL pulse to a transparent optical solid and diagnosing the ensuing material modifications remains a challenge (2).

By studying and understanding the interactions in materials that arise in nonlinear optics, steps can be taken to utilize material behavior in this ultrashort ultra-intense regime. If material responses and the ability of a material to maintain its native properties when subject to ULLs are well understood, the possibilities to both improve optical systems as well as acquire valuable information on an existing optical system can be realized.

1.1 History

Laser-induced breakdown and damage in transparent materials has been an area of study for over 50 years. Keldysh Theory, a fundamental backbone of numerous models including that which will be presented in this thesis, was developed by L. V. Keldysh in 1964 (3). This was about 30 years before the first true femtosecond laser prototypes were built and nearly 40 years before they were commercialized! It is truly amazing that his theory, published significantly before the time of the ultrashort ultra-intense laser, remains the most commonly accepted description of photoionization mechanisms in transparent materials to date.

To elaborate on what makes the work done by Keldysh such a substantial feat, one must look at the damage mechanisms at the timescale just above what is presently considered ultrashort. Specifically, this regime covers pulse durations longer than a few tens of picoseconds to nanosecond pulses. As is the case with ultrashort pulses, once sufficient energy is absorbed by the material, irreversible damage results. When the pulse width of the laser is on the timescale mentioned above, the absorbed laser energy is transferred by the material's excited electrons to its lattice. This results in a thermal diffusion of energy out of the focal volume ultimately leading to damage by means of melting and/or fracturing (1) (4). The rates of energy deposition and thermal diffusion together determine the damage threshold of the material which is now known to scale with the square root of the pulse duration (5).

Using pulses shorter than 10 ps, the first deviation from thermal damage effects was observed in 1984 by Soileau *et al* giving birth to a new regime: subpicosecond damage mechanisms (6). This created an entirely new realm of questions which led to study after study. Decoupling the absorption and lattice heating processes meant that electrons in the conduction band could be heated much faster than they could be

cooled through phonon emission (7). Only after the pulse has ended can the excited electrons transfer their energy to the lattice. This causes a "shock-like" deposition of energy on a time scale much shorter than thermal diffusion can occur, the result being a new form of damage in which the material experiences surface ablation or permanent structural change to the bulk (1).

From here, the journey to understand and acquire experimental data on laser induced damage and the underlying processes at play shifted focus to subpicosecond laser systems. Earlier, Keldysh Theory was mentioned. As this shift to ultrashort laser systems occurred, Keldysh Theory was also seen in new light. Finally, its power in modeling ionization mechanisms within condensed media began to be understood.

1.2 Challenges and Opportunities

Despite the long history, much can still be learned in the laser-induced damage field. The potential knowledge that remains sought after takes on even greater value when one considers the fact that laser systems continue to advance. Ultrashort pulses are becoming even shorter, as many research groups extend and refine the study of lasing in the subfemtosecond regime. Pursuits of new emission spectra have been successful in contributing to the number of unique frequencies at which lasing has been observed. These, along with other advancements in laser technology, will continue to create vacancies in the field that only further research can fill.

Aside from what future technology brings to the table, there are other challenges that remain when performing laser induced damage studies. Even after years of research, and with Keldysh Theory widely accepted, questions still exist pertaining to the relative role between ionization mechanisms of conduction band electrons. Measuring techniques continue to be explored when dealing with the time-resolved

excitation processes and thus measuring certain ultrafast nonlinear optical responses of materials have yet to be investigated in detail (8).

Another challenge in studying the damage behavior of transparent materials arises when these materials are subject to multiple femtosecond laser pulses. It is well known that the damage threshold fluence of materials under multi-pulse irradiation is lower compared to single-shot irradiation (9). This effect is often referred to as incubation and has been explained by the formation of self-trapped excitons (STEs) and subsequently color centers (9). The excitations can be long-lived with lifetimes on orders ranging from minutes to months at room temperature (10) (11).

Schaffer *et al* questioned whether surface damage thresholds are the same as bulk thresholds, or whether they are lower due to defects or surface states that are more easily ionized than the bulk (1). They conducted experiments to measure bulk thresholds of various materials, but results are not conclusive. In addition, very little theoretical work has been done that takes into account surface variables and the importance they may have on damage threshold.

1.3 Motivation

As the development of new laser systems advances, the desire to understand their effects on various optical systems follows suit. This is of particular interest to the different branches of military, where many of their devices and crafts rely on a wide variety of optical systems. Furthermore, it is relatively common knowledge that lasers already have an established role in a number of military applications. With the advancement of laser technology, new possibilities in weaponization and defense applications arise. It is of utmost importance to understand these potentials and take active measures in preserving security.

To understand the effects of a laser system on a material, one must look at the underlying absorption processes as many have done before. A strong understanding of the fundamentals behind absorption could result in the ability to predict the onsets of damage as laser parameters and materials themselves change. This could then stem active research in strengthening optical materials against certain laser systems. Even further, one may be able to use nonlinear response data to create"fingerprint" signals for various materials, providing the capability to reveal the composition of a target optical system.

This thesis investigates theory behind laser induced absorption phenomena, and uses this theory to construct a working model that is used to determine damage occurrences of a number of optical materials at various laser parameters.

Chapter 2

Laser Induced Damage

As mentioned, to understand laser induced damage of an optical material the damage mechanisms and electron processes that fuel them must be explained. Damage mechanisms in the picosecond-nanosecond regime were briefly described. At these pulse durations, electrons have sufficient time to transfer their absorbed energy to the lattice causing melting and fracturing. Thus, thermal diffusion is the damage mechanism, but what is the process that leads to it?

Laser technology advanced, and ultrashort took on new meaning when subpicosecond pulses were realized. Electrons no longer had time to deposit their absorbed energy into the lattice while exposed to these short pulses. Absorption now continues without thermal diffusion, and only after the pulse has ended can this immense amount of energy be transferred to the material. Ablation of the surface and permanent structural change of the material results.

The discovery of this new damage mechanism in the ultrashort regime had instant promise. This is largely due to intrinsic breakdown thresholds for materials in the picosecond-nanosecond regime being extremely difficult to determine and reproduce (12). Material damage produced by pulses on the femtosecond timescale was found

to be much more consistent. Short pulses require less energy than longer pulses to reach the intensity required for optical breakdown, and as a direct result of a lower deposited energy, precise material modifications opened new doors for micromachining (1). However, of interest to this thesis is if this deterministic breakdown behavior can be theoretically modeled as laser and material properties are altered.

There are two well established processes that exist to describe free-carrier generation in an optical material subject to an intense electromagnetic wave. These processes are (a) electron impact ionization and subsequent avalanching and (b) photoionization. Various laser and material parameters are used to determine the relative role each process has in contributing to material optical breakdown. Lastly, it should be stated that the generation of free-carriers must reach a critical electron density, N_{cr}, equal to 10^{21} [electrons/cm^3] for optical damage in a material to occur. This critical value is widely accepted in the field of laser-induced damage as the onset of breakdown.

2.1 Electron Impact and Avalanche Ionization

According to Jones (2) the origin of electron impact avalanche ionization can be traced back to founding work done in 1932 by von Hippel (13). A very early version of the electron-avalanche laser breakdown theory was developed by Yablonovitch and Bloembergen 40 years later (14). The theory has since undergone various significant revisions, but the basic concept remains.

Their theory was composed of three stages: initial electron excitation, plasma formation by means of electron avalanching, and energy deposition. Avalanche ionization is a process in which free carrier absorption leads to the ionization of additional carriers by impacting valence electrons. In order for avalanching to occur, there is a

necessity of what are referred to as "seed" electrons. These seed electrons are generated via photoionization through either defect and impurity electrons, or electrons in the valence band. Fig 2.1 describes the process.

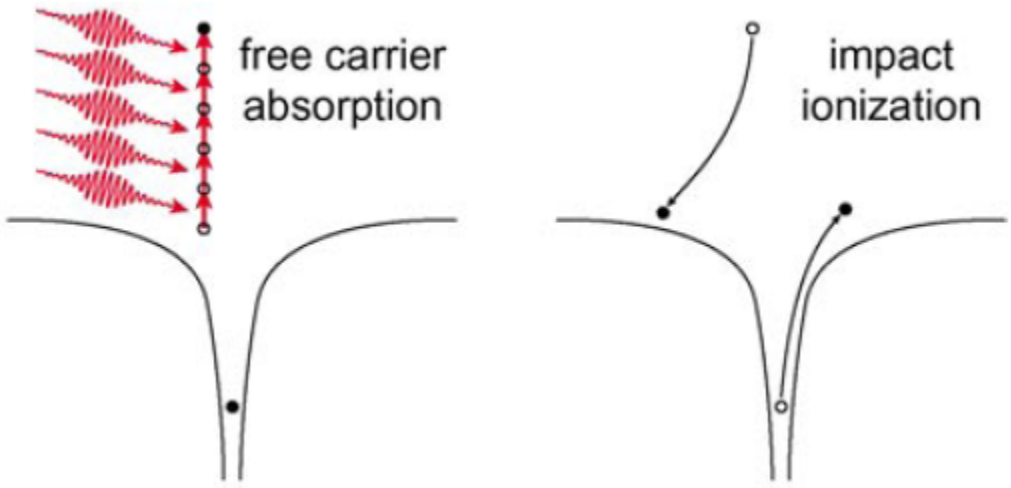

Figure 2.1: Schematic diagram of electron impact ionization by means of photoionization. A free electron is excited through photon absorption and ionizes an additional electron as soon as it has enough energy to do so (1).

Once electrons are excited into the conduction band they continue to absorb energy from the incident beam of photons. This linear photon absorption process results in conduction electrons with excess energy greater than that of the material band gap. When this energy is reached, the electron can then collisionaly ionize an additional electron from the valence band. Specifically, when n is the smallest number possible that satisfies $n\hbar\omega \geq E_g$ impact ionization occurs. Free carriers will continue absorbing energy and ionizing additional electrons as long as the laser field is present. According to Stuart *et al* (4) the electron density due to impact ionization, N, in the conduction band can be described by

$$\frac{dN}{dt} = \alpha I(t) N \tag{2.1}$$

where α is known as the avalanche coefficient. This model incorporates a flux doubling

approximation which implies that an electron in the valence band is ionized as soon as an electron in the conduction band has sufficient energy to do so. Thus, no electrons exist in the conduction band with energy higher than twice the band gap.

Avalanche ionization is an extremely efficient process. In the case of longer pulses, more time is available for the electron density growth which leads to material damage thresholds at laser intensity values much lower than what is seen at shorter pulses. The source of the seed electrons plays an important role as well. Over a long pulse, a material with a high concentration of defects can provide a significant amount of seed electrons. The material will damage much easier than a purer material, one of the reasons determining the breakdown threshold of materials using pulses greater than 10 ps is difficult (12). Depending on the density of impurities in a material, damage is often realized at laser intensities and frequencies much lower than that required for photoionization to occur.

At shorter pulses (subpicosecond regime), rather than existing defects or impurities, intrinsic material properties control damage behavior (9). At these shorter durations, photoionization results in what is commonly referred to as self-seeded avalanche ionization (4). Self-seeded avalanche makes short pulse breakdown much less dependent on defects allowing for deterministic material breakdown (15). If the right short pulse conditions are met, photoionization has the potential to dominate the ionization process and can optically damage a material without any contribution from avalanche ionization (1).

2.2 Photoionization

Photoionization refers to the direct excitation of electrons by a laser field (1). When a material's band gap energy exceeds that of a single photon of visible light, multi-

ple photons are required to excite an electron from the valence to conduction band. Photoionization provides the aforementioned"seed" electrons necessary for avalanche breakdown to occur for ultra-short pulses. Depending on the intensity and frequency of the incident pulse, there are two regimes of photoionization, multiphoton ionization and tunneling ionization. The total photoionization contribution to the electron density rate equation is

$$\frac{dN}{dt} = P(I) \tag{2.2}$$

where *P(I)* encompasses the contributions from both multiphoton and tunneling phenomena. The exact contribution of each process depends on material and laser parameters described within Keldysh Theory (3). Detailed explanation will be given within the modeling portion of this thesis.

2.2.1 Multiphoton Ionization (MPI)

Although the interaction probability for single-photon absorption in a laser-material system is highest, if two or more lower energy photons arrive simultaneously there is some probability that they will excite an electron within the material. The necessary condition to be satisfied is

$$(E_1 - E_0) \leq hc\left(\frac{1}{\lambda_1} + \frac{1}{\lambda_2} + ... + \frac{1}{\lambda_n}\right) \tag{2.3}$$

where λ_1 ... λ_n are the wavelengths of individual photons. If the total energy of the simultaneous incident photons is greater than the band gap, an electron is excited.

The probability of two-photon absorption is much smaller than that for single-photon absorption, and the probability of three-photon absorption is smaller still (16). However, the absorption probability is a nonlinear process and experiences an

increase proportional to I^n where n refers to n-photon absorption. For example, the probability of three-photon absorption increases with intensity as I^3. Fig 2.2 shows the multiphoton ionization process.

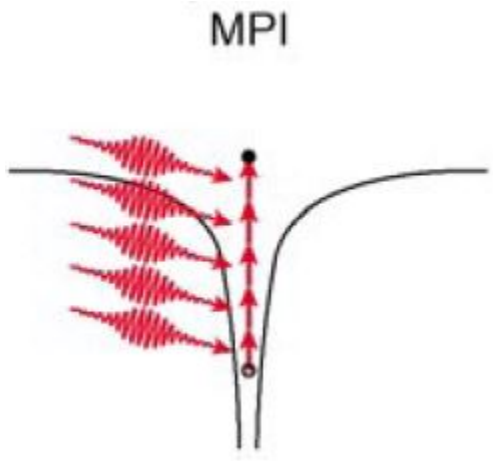

Figure 2.2: Schematic diagram of electron excitation due to multiphoton ionization. (1).

2.2.2 Tunneling Ionization

Tunneling ionization is the second form of photoionization that occurs within a material. In the presence of a strong electric field, the Coulomb potential that binds a valence electron to its atom is suppressed substantially. As the electric field becomes stronger, this barrier can be suppressed enough so that the energy deposited by an incident photon results in an electron tunneling through the reduced barrier (17). These electrons are now free and may serve as "seed" electrons for avalanche ionization. Fig 2.3 shows the tunneling ionization process.

It is also necessary to point out that an intermediary period exists where the photoionization process transitions from MPI to Tunneling. In this region, photoionization is a combination of both processes. Fig 2.4 demonstrates the joint ionization contributions.

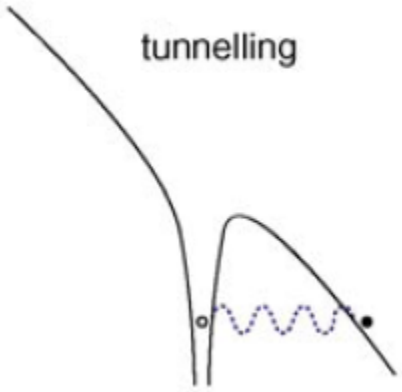

Figure 2.3: Schematic diagram of electron excitation due to tunneling ionization. A strong electric field is required to sufficiently reduce the Coulomb barrier and induce tunneling. (1).

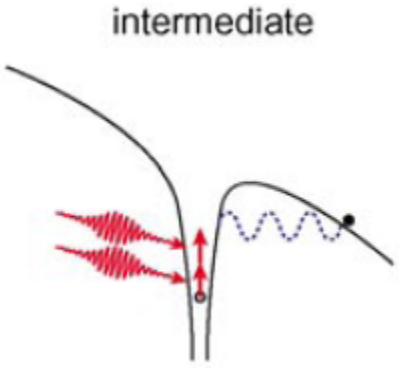

Figure 2.4: Schematic diagram of electron excitation due to both MPI and tunneling ionization. An electron first absorbs energy through MPI and subsequently tunnels through the reduced barrier. (1).

Chapter 3

MATLAB Modeling of Absorption Phenomena

Now that the mechanisms and associated ionization processes behind laser induced damage have been described, it is time to delve into how the behavioral model operates. First, it is restated that a critical electron density, N_{cr}, equal to 10^{21} [electrons/cm^3] is necessary to induce optical breakdown within a material. For a set of particular laser and material input parameters, the model will predict an electron density growth. Comparing the final density value of this growth to the critical electron density value above will serve as the means to determine whether damage has occurred. The critical electron density will also serve as the reference for model accuracy tests done in the experimental portion of this thesis.

MATLAB served as the platform for this model. It is an excellent tool for modeling and simulations, as many functions and mathematical operations are built in for easy access. This chapter will present an oversight of what drives the model functionality and the inputs required. The full source code for the model can be seen in the appendix. It is again noted that this model was built in collaboration with Dr. Troy

Alexander. His contribution as well as guidance were key to the development of a functioning model.

3.1 Model Inputs

The model consists of a main script accompanied by various role specific scripts that are called upon as necessary. Before the behavioral expressions within these scripts are presented and explained, a list of material and laser parameters needed for the calculations and model execution will be provided. These parameters are passed between scripts as required.

3.1.1 Material Parameters

The material input parameters are handled by a separate script named *Material Flag*. Within the main script, **matFlag** is a defined variable used to select a particular material within the *Material Flag* script. Once a material is selected, the script returns each material parameter to be used in subsequent portions of the model. The material parameters provided by the script, as well as each available material choice for variable **matFlag**, can be seen in Table 3.1.

Avalanche coefficient, effective electron mass, and effective decay constants were obtained from the literature where available. Due to differences in thin film fabrication techniques and environments, these material values may vary from film to film. However, only the effective decay constant was seen to fluctuate on a scale exceeding single-order magnitude (12). In order to create as accurate a model as possible, these model parameters should be fit to experimental results once those results are acquired. The additional material properties of this model may be measured using various instrumentation or obtained from well established literature.

Table 3.1: Model Input Information: Materials

Available Materials	Material Input Parameters	Description
Fused Silica (delta eV = 9)	alpha	Avalanche Coefficient [cm^2/J]
Fused Silica (delta eV = 7.5)	delta eV	Material Band Gap [eV]
GaAs	me	Effective Electron Mass [kg]
ZnSe	n0	Linear Refractive Index
Ge	n2	Non-Linear Refractive Index
HfO_2	T	Effective Decay Constant [fs]
TiO_2		
Ta_2O_5		
Al_2O_3		
SiO_2		

The Sellmeier Equation is used to calculate refractive index for nearly all of the available materials within the model. This equation takes advantage of an empirical relationship between the refractive index of optical materials and the wavelength of light. The usual form of the equation for optical materials is

$$n^2(\lambda) \equiv 1 + \frac{B_1\lambda^2}{\lambda_2 - C_1} + \frac{B_2\lambda^2}{\lambda_2 - C_2} + \frac{B_3\lambda^2}{\lambda_2 - C_3} \tag{3.1}$$

where n is the refractive index, λ is the laser wavelength, and $B_{1,2,3}$ and $C_{1,2,3}$ are experimentally determined Sellmeier coefficients. The Sellmeier equations pertaining to each material were obtained using an online refractive index database (18). When a Sellmeier equation was not readily available, other research was done to obtain initial refractive index values for these materials. Again, to increase accuracy, the refractive

index of a material and sample of interest may be measured and incorporated into the model. The Sellmeier equation was used to provide a quick method to alter laser parameters and simultaneously account for the changes of refractive index in a material.

3.1.2 Laser Parameters

After a material is selected, it is common to constantly alter the laser properties and monitor the effects on electron density growth behavior of that material. Due to this fact, the laser property inputs are handled within an individual section of the main script for easy access. These parameters can be seen in Table 3.2.

Table 3.2: Model Input Information: Laser System

Laser Input Parameters	Description
lambda (λ)	Laser Wavelength [µm]
omega (ω)	Radial Frequency [rad/s]
T _FWHM (τ_{FWHM})	Full Width Half Maximum Pulse Duration [fs]
tau (τ)	Time at which irradiance is $1/e^2$ of peak value [fs]
I_0	Peak Laser Intensity [W/cm^2]
P	Laser Power [mW]
R	Laser Repetition Rate [Hz]
w_0	Beam Radius [m]

Of note, if the peak laser intensity I of the laser system is known, laser power P, beam radius w_0, and repetition rate R are not required as inputs. Otherwise, these parameters are required in order for the model to perform a calculation of the peak laser intensity. The calculation process is as follows:

$$I_0 = \frac{4E_p}{\tau w_0^2 \pi \sqrt{2\pi}} \qquad [\mathrm{W/m^2}] \quad (3.2)$$

Where

$$E_p = \frac{P}{R} \quad \text{[J]} \quad (3.3)$$

is the pulse energy in Joules. This relationship is derived by inserting the laser pulse equation into the following equation applicable for radially symmetric beams:

$$E_p = \int_{-\infty}^{+\infty} \int_{0}^{2pi} \int_{0}^{+\infty} I(r,t) r dr d\theta dt \quad \text{[J]} \quad (3.4)$$

For the case that gives the result seen in equation 3.2, the laser pulse *I(r,t)* is a Gaussian pulse of the form:

$$I(r,t) = I_0 exp\left(-2\frac{r^2}{w_0^2}\right) exp\left(-2\frac{t^2}{\tau^2}\right) \quad \text{[W/m}^2\text{]} \quad (3.5)$$

where I_0 is the peak irradiance, τ is the time at which the irradiance is $1/e^2$ of the peak value I_0, and w_0 is the beam radius at which the irradiance is $1/e^2$ of the peak value I_0. Full derivations and additional details regarding the relationships between pulse fluence and pulse power for an arbitrary radially symmetric beam can be seen in reference (19).

3.2 Electron Density Rate Equations

Stated at the start of this thesis, Keldysh theory is used as a fundamental backbone to model electron density growth via photoionization processes. Keldysh shows that multiphoton ionization and tunneling ionization can be demonstrated within the same framework (3). However, as demonstrated earlier, the conceptual picture of these processes varies significantly, as will the calculations and approximations used to model them. Thus, to see the significance of their individual roles and behavior under

different laser parameter scenarios, these processes are first modeled apart from one another through the use of separate MATLAB scripts.

Stuart *et al* developed a theory for electron density growth due to avalanche ionization as seen in equation 2.1 (4). The theory includes assumptions of both a flux-doubling approximation, and also a constant electron energy distribution in the conduction band as the electron density grows. Overall, it is a much simpler ionization mechanism to model as opposed to photoionization.

Combining these ionization mechanism theories, the total electron density rate equation becomes:

$$\frac{dN}{dt} = \alpha I(t)N + P(I) \tag{3.6}$$

Where αIN represents the avalanche contribution and *P(I)* represents the photoionization rate. This rate equation smoothly highlights the transition between two ionization extremes. Photoionization takes place primarily at the peak of the pulse where the intensity, and thus photon flux, is the highest. After the peak passes, photoionization becomes relatively unimportant and electrons excited at the peak serve as seeds for avalanche ionization.

Of note, this model allows for the inclusion of an additional term, -$\frac{N}{T}$, to the total rate equation, T being the effective relaxation time. Effective relaxation is a broad term in this sense, accounting for all of the various forms of recombination mechanisms. This term is of interest when relaxation timescales are significant relative to the incident pulse duration. Plans to investigate the effects of this term as well as exact relaxation phenomena have been addressed in the scope of future work portion of this thesis.

3.2.1 Tunneling Ionization Rate Equation

Tunneling ionization is the dominant photoionization process at low laser frequencies and strong electromagnetic fields. In this case, the behavior of the ionization probability is reduced to equation (40) of Keldysh (3). Keldysh's relationship for the electron tunneling rate with no MPI contribution is as follows:

$$W_{tun} = \frac{2}{9\pi^2}\frac{E_g}{\hbar}\left(\frac{m_e E_g}{\hbar^2}\right)^{3/2}\left(\frac{e\hbar F}{m_e^{1/2}E_g^{3/2}}\right)^{5/2} \times exp\left[-\frac{\pi}{2}\frac{m_e^{1/2}E_g^{3/2}}{e\hbar F}\left(1-\frac{1}{8}\frac{m_e\omega^2 E_g}{e^2F^2}\right)\right] \tag{3.7}$$

Here E_g is material band gap, m_e is material electron effective mass, e is electron charge, and ω is the radial frequency of the incident light. F represents the Electric Field Strength and is calculated from the following equation seen in reference (20):

$$F = \sqrt{\frac{2I}{cn\epsilon_0}} \tag{3.8}$$

Here, I is peak laser intensity, n is refractive index, and ϵ_0 is the permittivity of free space.

3.2.2 Multi-Photon Ionization Rate Equation

The second form of photoionization has been described as multi-photon ionization. At higher laser frequencies and lower electromagnetic fields, this nonlinear ionization process will occur. Direct excitation of an electron is observed after a simultaneous absorption of several photons. The exact number needed is found by satisfying equation (2.3) for a particular material of interest. The photoionization rate for MPI is

presented as equation (41) in Keldysh (3) and is as follows:

$$W_{MPI} = \frac{2}{9\pi}\omega\left(\frac{m_e\omega}{\hbar}\right)^{3/2}\phi\left[\left(2\left(\frac{E_g^*}{\hbar\omega}+1\right)-\frac{2E_g^*}{\hbar\omega}\right)^{1/2}\right] \times exp\left[2\left(\frac{E_g^*}{\hbar\omega}+1\right)\left(1-\frac{e^2F^2}{4m_e\omega^2E_g}\right)\right] \times\left(\frac{e^2F^2}{16m_e\omega^2E_g}\right)^{(E_g^*/\hbar\omega+1)} \tag{3.9}$$

Where E_g^* is the effective ionization potential given by

$$E_g^* = E_g + \frac{e^2F^2}{4m_e\omega^2} \tag{3.10}$$

ϕ represents Dawson's Integral and is given by

$$F(x) = e^{-x^2}\int_0^x e^{-t^2}dt \tag{3.11}$$

There are two ways to calculate the Dawson integral within MATLAB. The first way is by utilizing *mfun* which is supplied through MATLAB's symbolic math toolbox and can be used to call the Dawson integral. This method was found to be extremely time consuming. The other method is through the utilization of dawson.m, a MATLAB file created by Peter Acklam and acquired through MATLAB File Exchange (21). This proved to be a much more efficient means in calculating the multi-photon ionization rate.

3.2.3 Keldysh Parameter and Full Rate Equation

The two cases, MPI vs Tunneling Ionization, make up the two regimes of photoionization. However, simply combining the two reduced equations will not yield the correct full rate equation needed to model electron density growth over the transition

between these two regimes. To describe this transition, an expression developed by Keldysh is introduced and is appropriately known as the Keldysh parameter (3):

$$\gamma = \frac{\omega}{e}\left[\frac{m_e c n \epsilon_0 E_g}{I}\right]^{1/2} \tag{3.12}$$

Here ω is again radial frequency, e is electron charge, m_e is material electron effective mass, c is the speed of light, n is the material's refractive index, ϵ_0 is the permittivity of free space, E_g is band gap, and I is peak laser intensity.

The value of this parameter determines whether photoionization is dominated by tunneling or by multi-photon absorption, or if there is a contribution from both. The key value is 1.5. When the Keldysh parameter falls below 1.5, photoionization is a tunneling process. Above 1.5, photoionization is a multi-photon process. The intermediate regime where both tunneling and MPI contribute occurs when the parameter is near or equal to 1.5, and it is here that the full rate equation is necessary to describe the photoionization behavior. Fig 3.1 combines images presented earlier in this thesis to demonstrate photoionization as the Keldysh parameter varies.

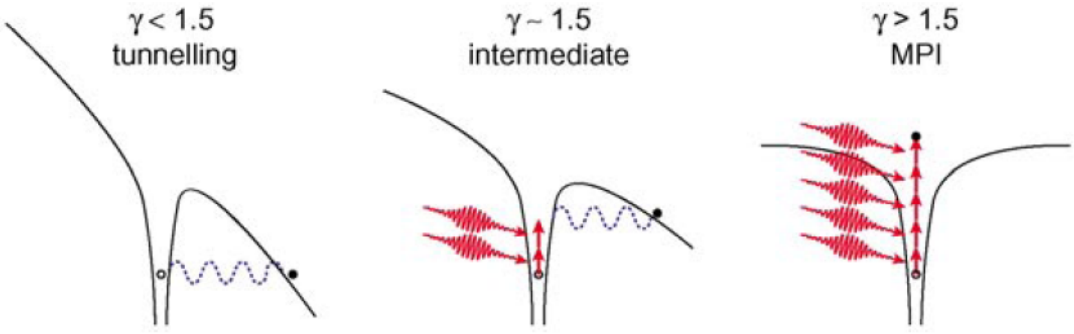

Figure 3.1: Schematic diagram of the photoionization of an electron in an atomic potential for different values of the Keldysh parameter (1).

Through use of the Keldysh parameter, the full ionization probability was developed. The full rate equation for photoionization is given as equation (37) in Keldysh

(3) and is as follows:

$$W_{full} = \frac{2\omega}{9\pi}\left(\frac{\sqrt{1+\gamma^2}}{\gamma}\frac{m_e\omega}{\hbar}\right)^{3/2} Q\left(\gamma, \frac{E_g^*}{\hbar\omega}\right) \times$$
$$exp\left\{-\pi\left(\frac{E_g^*}{\hbar\omega}+1\right)\times\left[K\left(\frac{\gamma}{\sqrt{1+\gamma^2}}\right)-E\left(\frac{\gamma}{\sqrt{1+\gamma^2}}\right)\right]/E\left(\frac{1}{\sqrt{1+\gamma^2}}\right)\right\} \tag{3.13}$$

Q in equation (3.13) refers to a function described in Keldysh as:

$$Q(\gamma, x) = \left[\pi/2K\left(\frac{1}{\sqrt{1+\gamma^2}}\right)\right]^{1/2}$$
$$\times\sum_{n=0}^{\infty} exp\left\{-\pi\left[K\left(\frac{\gamma}{\sqrt{1+\gamma^2}}\right)-E\left(\frac{\gamma}{\sqrt{1+\gamma^2}}\right)\right]n/E\left(\frac{1}{\sqrt{1+\gamma^2}}\right)\right\} \tag{3.14}$$
$$\times\phi\left\{\left[\pi^2(2\langle x+1\rangle - 2x + n)/2K\left(\frac{1}{\sqrt{1+\gamma^2}}\right)E\left(\frac{1}{\sqrt{1+\gamma^2}}\right)\right]^{1/2}\right\}$$

Only variable E_g^* takes a new form in the full rate equation. All other variables have been presented and described within equations (3.7) and (3.9). The effective band-gap, E_g^*, becomes:

$$E_g^* = \frac{2}{\pi}E_g\frac{\sqrt{1+\gamma^2}}{\gamma}E\left(\frac{1}{\sqrt{1+\gamma^2}}\right) \tag{3.15}$$

In equations (3.13), (3.14), and (3.15), K and E are complete elliptic integrals of the first and second kind. These elliptic integrals are handled by the tool *ellipke* in MATLAB.

It has already been presented that photoionization is key to material breakdown in the subpicosecond regime whether directly producing a critical electron density itself or by providing "seed" electrons for subsequent avalanche ionization. Thus,

the full rate photoionization equation, equation (3.13), is the most important tool in modeling the electron density growth.

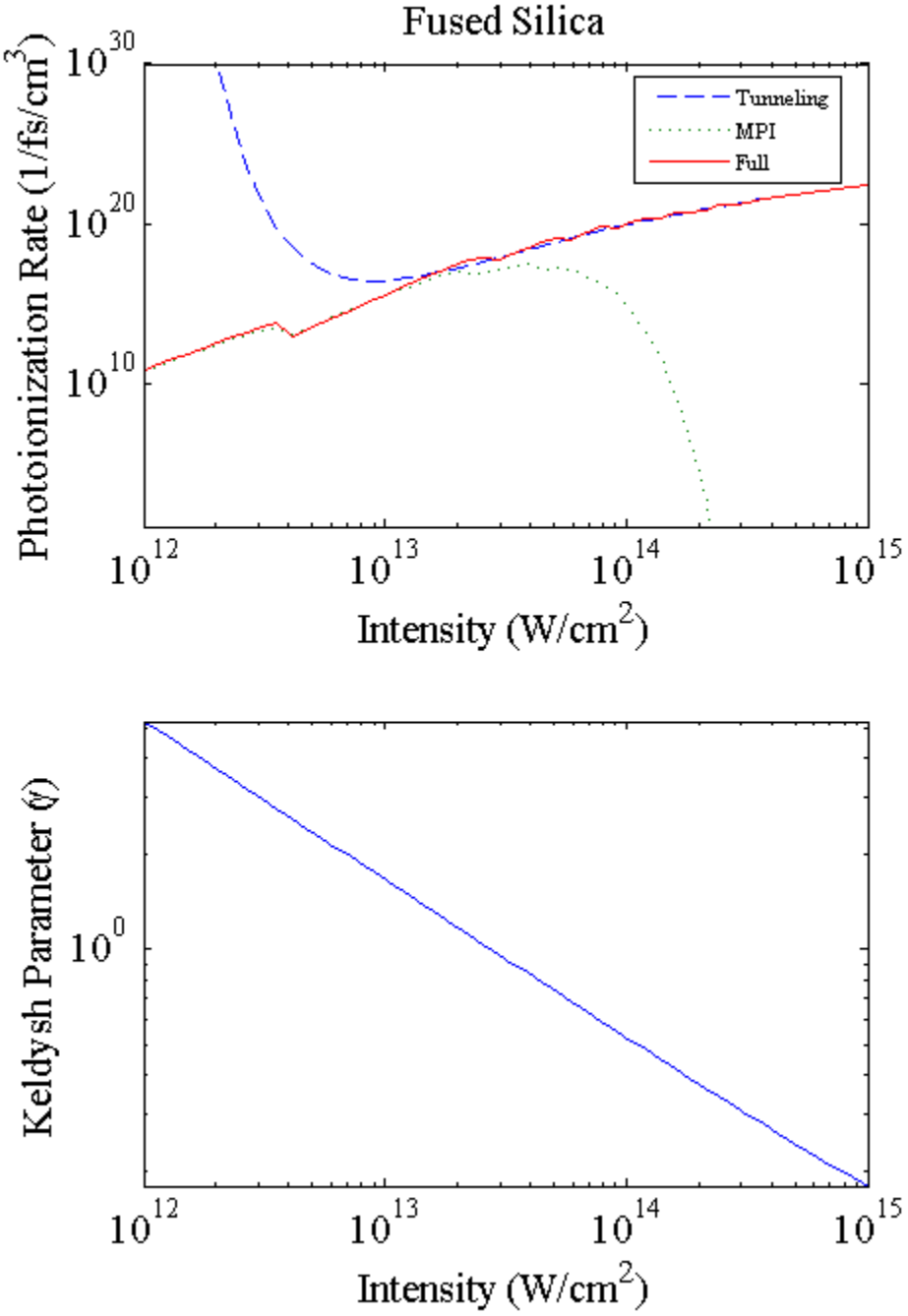

Figure 3.2: Photoionization Rate and Keldysh parameter as a function of laser intensity at $\lambda = 800$ nm and pulse duration 80 fs. The material demonstrated is Fused Silica (9 eV band-gap). In the top image, the dashed line represents the Tunneling Ionization Rate, the dotted line represents the MPI Rate, and the solid line is the Full Photoionization Rate. Note that the two separate rates overlap at a Keldysh parameter of about 1.5.

In Fig (3.2) the tunneling rate, multi-photon rate, and full photoionization rate are shown as a function of laser intensity for 800 nm light and pulse duration 80 fs. The material used in this simulation was Fused Silica (band-gap of 9 eV). Also in this figure, the Keldysh parameter is shown versus intensity. It can be seen from this figure that the full rate only agrees with the MPI rate for a Keldysh parameter above 1.5. Furthermore, the full rate agrees solely with the tunneling rate for a Keldysh parameter below 1.5. The full rate clearly avoids the respective over and underestimates introduced by these separate regimes. When observing the progression of the full rate as intensity increases, a step-like behavior is observed. This is due to the abrupt changes in the MPI process as intensity is varied. For example, at an intensity just below 4×10^{12} Wcm^{-2} MPI for Fused Silica changes from a 6-photon process to a 7-photon process (22). This is due to the increase of the effective band-gap with higher laser intensities. Simulations for other materials and various laser parameters consistently show an sudden transition between tunneling and MPI regimes at a Keldysh parameter near 1.5.

3.2.4 Avalanche Rate

Stated earlier, avalanche ionization is a much simpler process to model as shown by Stuart *et al* (4). Once "seed" electrons are created within the conduction band by photoionization, and a sufficient electric field remains present, the continuous linear absorption of several photons will eventually lead to electrons with enough energy to impact ionize additional electrons. Again, free carrier absorption will continue for the duration of the laser field. Therefore, as pulse duration is increased, avalanche can play an increasingly significant role in electron density growth. Keep in mind, though pulse duration may have this effect, avalanche ionization depends highly on

laser intensity. If a sufficient field is not present, pulse duration may have little to no role on carrier generation. This will be shown later.

For clarity, the equation for avalanche impact ionization, equation 2.1, is shown again below:

$$\frac{dN}{dt} = \alpha I(t) N \tag{3.16}$$

To obtain the constant avalanche coefficient α for a particular material, a fit is usually performed (12) (1). Others have solved a full kinetic equation to obtain the avalanche coefficient determined by scattering rates and the band gap of the material (7). The model in its present state uses a values obtained from literature until additional experimental data is acquired.

Fig 3.3 shows the electron density growth in fused silica (band-gap of 9 eV) when irradiated by 800 nm light for 300 fs. The peak intensity used for this simulation is $5{\times}10^{12}$ Wcm^{-2}. This is a scenario demonstrating significant contribution of avalanche ionization. Photoionization produces an electron density of about 10^{11} electrons/cm^3 at the peak of the pulse. Avalanche then takes over and by the end of the pulse, the total electron density reaches a value of over 10^{18} electrons/cm^3. To demonstrate the affect pulse duration can have on the contribution of avalanche, Fig 3.4 shows fused silica again irradiated by 800 nm light at an intensity of $5{\times}10^{12}$ Wcm^{-2} but for a duration of only 50 fs. Here, the end of the pulse shows that avalanching increased the electron density initially produced by photoionization by less than 10. However, the 300 fs pulse showed an electron density contribution due to avalanche ionization nearly 20 million times the photoionization induced density!

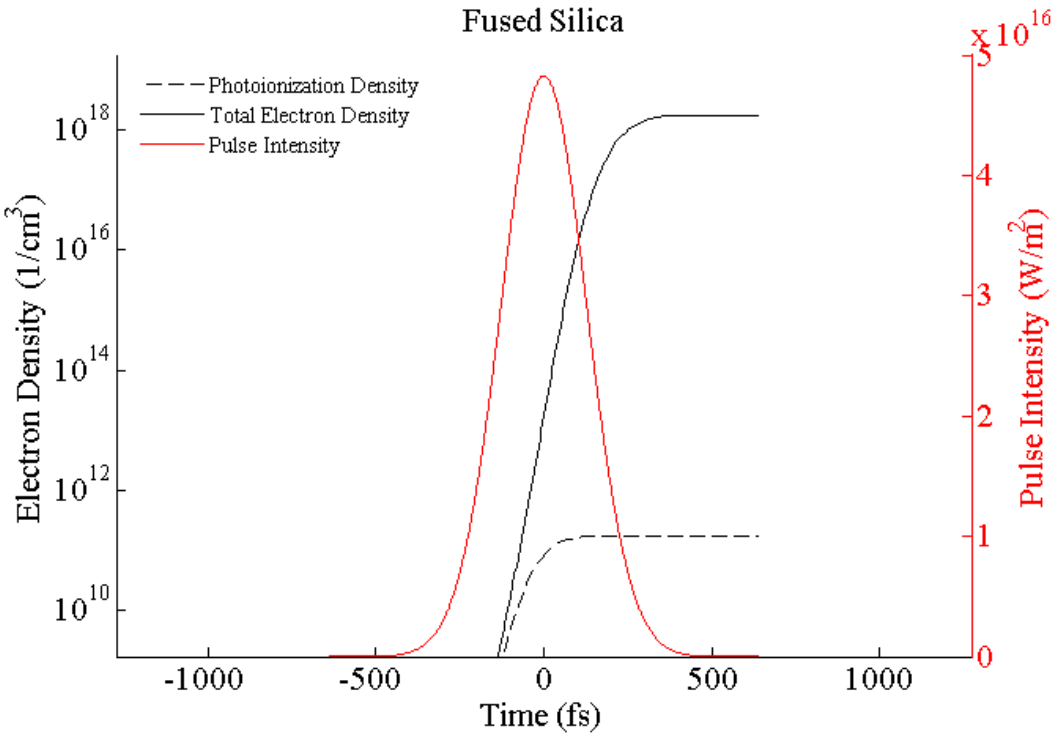

Figure 3.3: Model simulation of Fused Silica (band-gap 9 eV) irradiated by 800 nm light for 300 fs at an intensity of 5×10^{12} Wcm^{-2}. Of note is the significant role avalanche plays after photoionization introduces "seed" electrons.

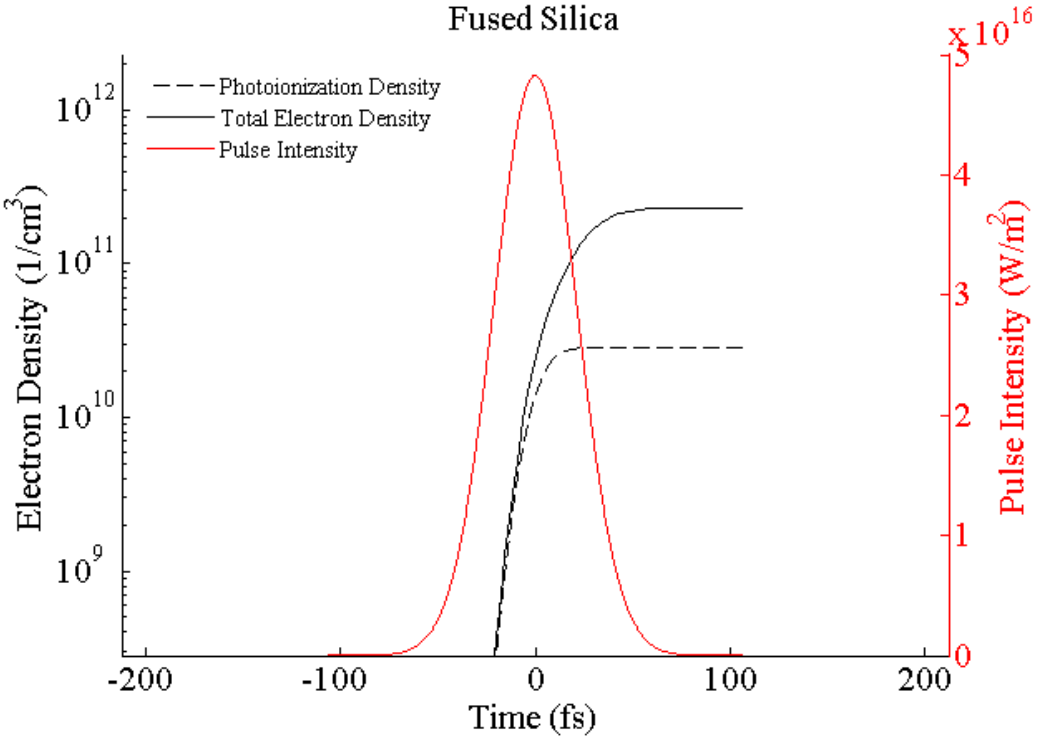

Figure 3.4: Model simulation of Fused Silica (band-gap 9 eV) irradiated by 800 nm light for 50 fs at an intensity of 5×10^{12} Wcm^{-2}. Here, avalanche plays a much smaller role in the total electron density growth.

Mentioned before, in some cases increasing the pulse duration will not result in an increased contribution of avalanche ionization. Stuart *et al* shows that avalanche ionization is not significant regardless of pulse duration if the threshold fluence of the material of interest is small, i.e., on the order of 0.2 J/cm^2 (7). Below this fluence, photoionization is almost completely responsible for optical breakdown. Again, this again is due to avalanche ionization's strong dependence on pulse intensity. Without the presence of a strong field, sufficient band bending will not occur and thus avalanching cannot be sustained.

Fig 3.5 and Fig 3.5 show simulations of GaAs (band-gap 1.42eV) irradiated by 800 nm light with an intensity of 1×10^{10} Wcm^{-2} for 50 fs and 1 ps respectively. In both cases, avalanche ionization is a non factor in total electron density growth

demonstrating no dependence on pulse duration.

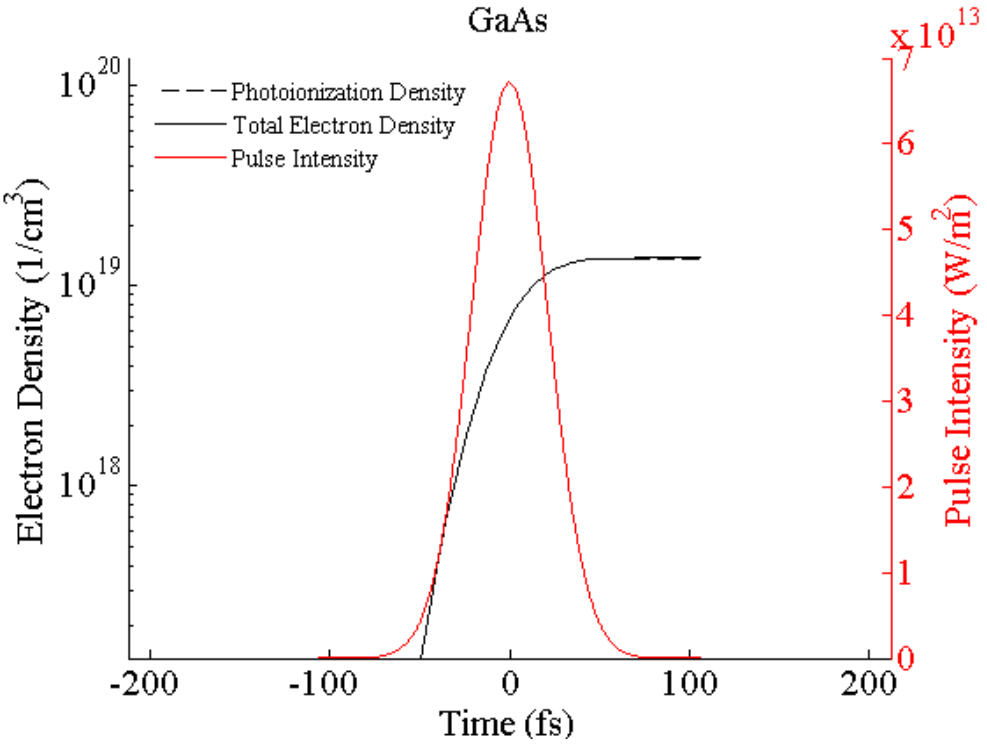

Figure 3.5: Model simulation of GaAs (band-gap 1.42eV) irradiated by 800 nm light for 50 fs at an intensity of 1×10^{10} Wcm^{-2}. Photoionization alone contributes to the electron density growth.

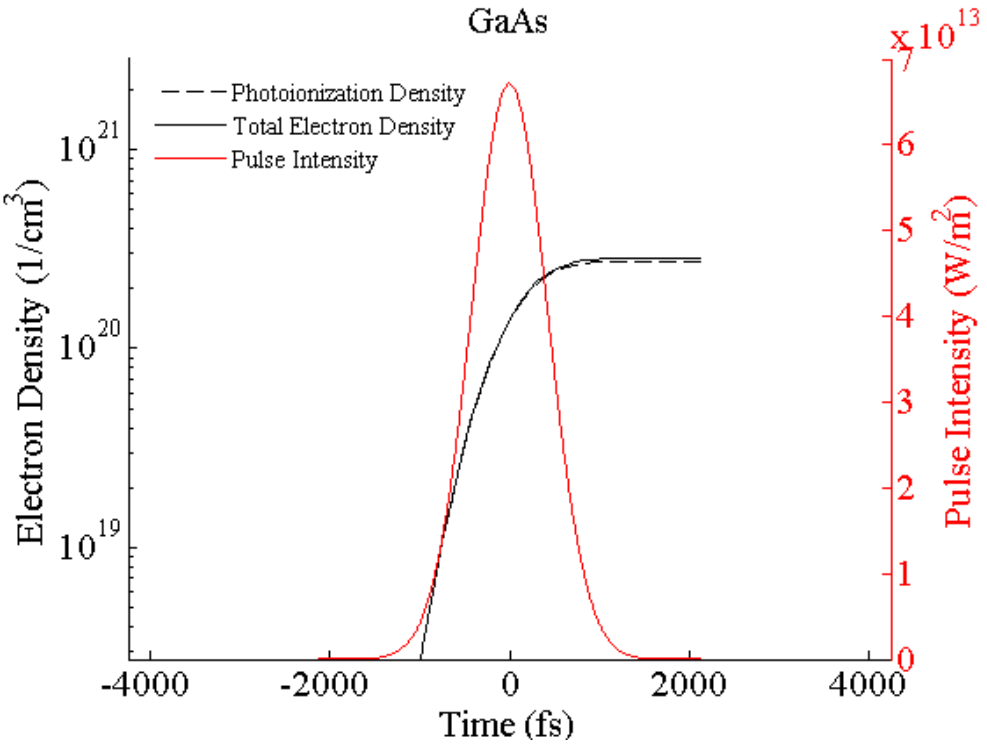

Figure 3.6: Model simulation of GaAs (band-gap 1.42eV) irradiated by 800 nm light for 1 ps at an intensity of 1×10^{10} Wcm^{-2}. Again, photoionization alone contributes to the electron density growth.

Chapter 4

Model Simulation Versus Experimental Results

Up to this point, a theoretical model that predicts electron density growth in optical materials due to laser excitation has been presented. The theory that drives this model, specifically the ionization mechanisms at play, led to the development of the rate equations. Both the theory and rate equations have been explained in detail. However, the accuracy of this model remains unproven. This chapter tests the strength of the model versus experimental results.

4.1 Gallium Arsenide

Thus far, Gallium Arsenide is the only material studied to test the accuracy of this model. The means by which the damage threshold was obtained experimentally and subsequent verification of this threshold using the theoretical model will be explained. Lastly, it should be noted that the photoionization process in the experiment and modeling for Gallium Arsenide was a single photon process. Due to many questioning

whether Keldysh's theory is valid for low photon multiplicity, Vaidyanathan *et al* compare Keldysh theory with perturbation formulas for one-photon absorption (23). They simplify Keldysh's MPI rate equation by assuming single photon absorption and then compare the resulting one-photon absorption coefficient to conventional first-order perturbation theory. They found that the Keldysh one-photon absorption edge agrees very well with that predicted by perturbation theory, i.e. within an order of one. Furthermore, they mention that Narducci *et al* (24) accurately predicted the frequency dependence and numerical values of the one-photon absorption coefficients in multiple materials at both the absorption edges and away from them using Keldysh Theory.

4.1.1 Finding the Damage Threshold Experimentally

Determining the laser ablation threshold of a material can be done in a variety of ways. A simple and well established technique that involves relating the size of the damage site to the incident laser fluence was chosen (25) (26) (27). This method predicts that for a Gaussian spatial beam fluence profile with $1/e^2$ laser beam radius w_0,

$$F(r) = F_0 exp\left(-\frac{2r^2}{w_0^2}\right) \tag{4.1}$$

Here F_0 is the peak laser fluence at the center of the crater. The laser ablated crater diameter is related to the the peak laser energy and ultimately threshold energy by the following equation,

$$D^2 = 2w_0^2 ln\left(\frac{F_0}{F_{th}}\right) = 2w_0^2 ln\left(\frac{E_p}{E_{th}}\right) \tag{4.2}$$

Here E_p is the pulse energy and is related to F_0 by

$$F_0 = \left(\frac{2E_p}{\pi w_0^2}\right) \tag{4.3}$$

In order to find the threshold intensity value for GaAs, single-shot laser pulses were taken at varying pulse energies on a GaAs sample. The diameter of the ablation craters were then measured using SEM imaging. Following the method laid out in Semaltianos *et al* (27), D^2 versus Ln(E_p) was plotted. From the slope of the least square fitted line to the data points, the exact beam radius was determined. Next, the x-intercept was found giving the pulse energy at the onset of ablation (D=0). Using this pulse energy threshold value and the laser pulse duration, the laser ablation intensity for GaAs was calculated using Eq 3.2. This equation is shown again below for clarity.

$$I_0 = \frac{4E_p}{\tau w_0^2 \pi \sqrt{2\pi}} \qquad [\mathrm{W/m^2}] \tag{4.4}$$

Fig 4.1 shows four damage sites to a GaAs sample. The outermost diameter (larger value) of each crater was chosen for calculations. Table 4.1 shows each pulse energy and corresponding crater diameter used for calculation. Finally, Fig 4.2 shows the graph of the crater diameter squared D^2 versus the natural log of pulse energy Ln(E_p). The fitted line to the experimental data was found to be

$$y = 32843x - 157367 \tag{4.5}$$

Extrapolation to the x-intercept results in a pulse energy threshold of 4.79149 μJ. From here, the threshold fluence was found to be F_{th} = .018575 [J/cm^2]. Finally, for a single-shot pulse of duration 80 fs and wavelength 800 nm, the damage threshold intensity for GaAs was determined to be I_{th} = **4.3626e11** [W/cm^2]. Of note, a

discovery was later made within the excel file that performed these calculations. This will be addressed in the following section.

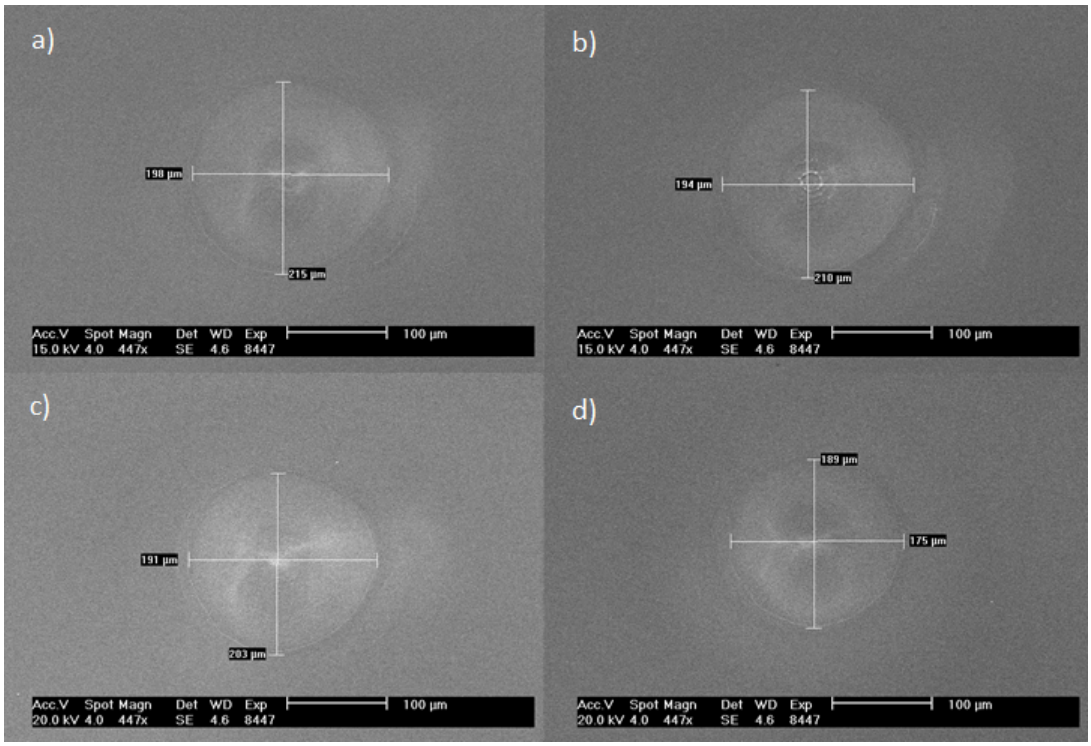

Figure 4.1: SEM images of single-shot ablation craters on GaAs. Gaussian pulses of duration 80 fs, $\lambda = 800$ nm, beam radius $w_0 = 90.613$ μm, and pulse energy $E_p =$ a) 500 μJ, b) 480 μJ, c) 440 μJ, and d) 400 μJ.

Table 4.1: GaAs: Ablation Crater Diameter with Varying Pulse Energy

Pulse Energy [μJ]	Outer Crater Diameter [μm]
680	239
660	234
640	235
620	234
600	229
580	239
560	221
540	217
520	219
500	215
480	210
460	210
440	203
420	203
400	197
380	189
360	189
340	188
320	191
300	171
280	163
260	158
240	152
220	146
200	140
180	117

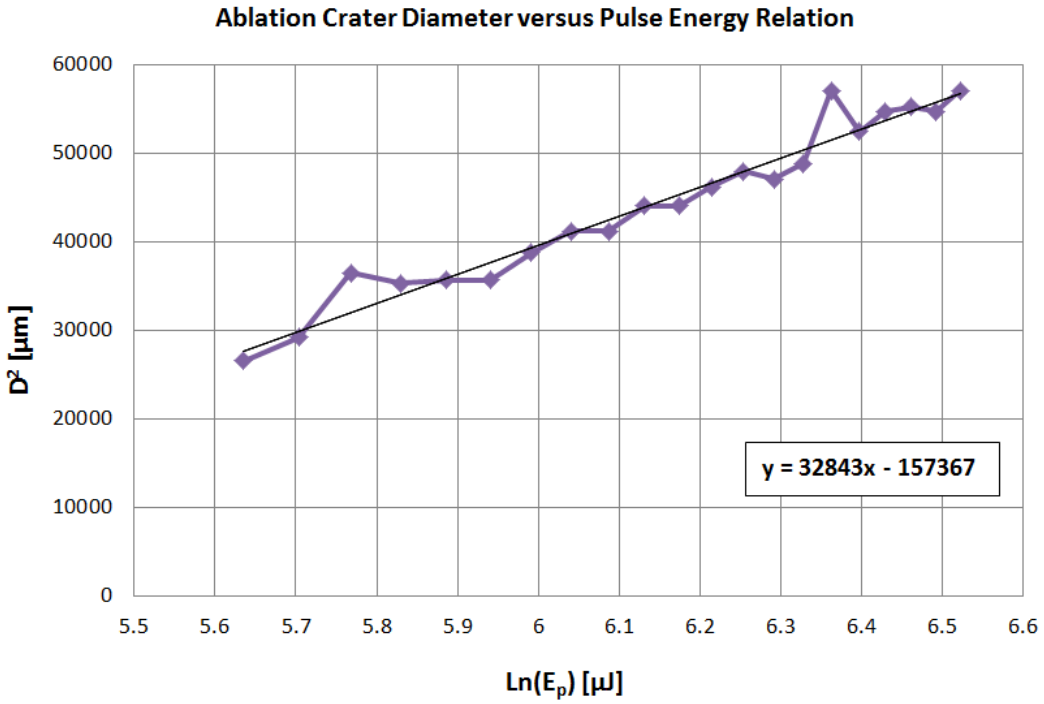

Figure 4.2: Graph of ablation diameter squared D^2 [μm] versus the natural log of pulse energy $Ln(E_p)$ [μJ]. All pulses were of duration 80 fs and wavelength 800 nm. The equation for the least squares fitted line is shown with the data.

4.1.2 Experimental Results versus Theoretical Predictions

With an experimental threshold intensity value found for GaAs, it was time to compare this to the theoretical predictions of the model. Again, the experimentally determined threshold intensity was found to be **4.3626e11** [W/cm^2] for a single-shot pulse of duration 80 fs and wavelength 800 nm, but was later discovered to be the result of inaccurate calculations. Using these laser parameters as inputs and selecting GaAs within the model, the total electron density was predicted to be N_D = **1.00458e21** [electrons/cm^3]. This resulted in an error under 1%, 0.458% to be exact, of the accepted critical electron density for damage onset N_{cr} = 1e21 [electrons/cm^3]. Fig 4.3 shows the model simulation of the electron density growth curve for the predicted damage scenario.

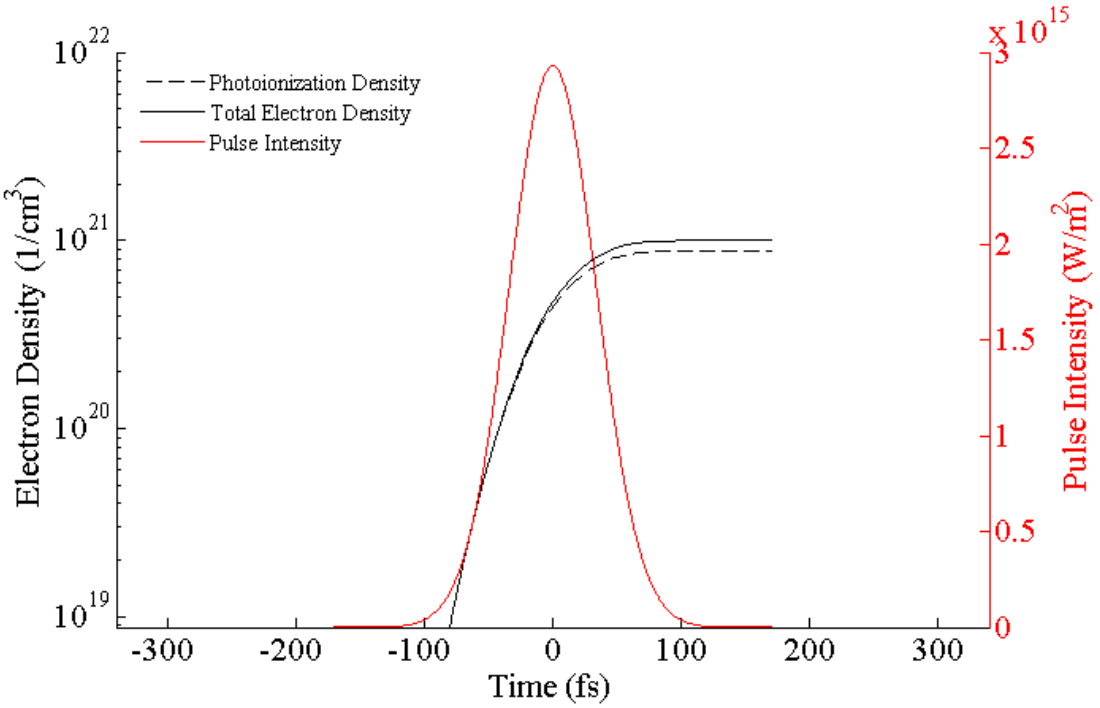

Figure 4.3: Model simulation of GaAs (band-gap 1.42eV) irradiated by 800 nm light for 80 fs at an intensity of 4.3626×10^{11} Wcm^{-2}. This results in a total electron density of N_D = 1.00458e21 [electrons/cm^3].

Unfortunately, due to the extreme correlation between the theoretical prediction and the experimental threshold value, no thought was given to the possibility of error during experimental calculations. Ensuing corrections, calculations using the experimental data presented earlier were redone, and a threshold intensity of **1.09697e13** [W/cm^2] was found. The predicted electron density, N_D, using this threshold intensity was determined to be **1.587e24** [electrons/cm^3], three orders of magnitude larger than seen originally and more importantly, three orders of magnitude larger than the accepted critical electron density value. Determining whether this discrepancy was due to errors in the model or to experimental procedures became the utmost priority.

Additional research was performed to better understand the methods utilized in experimentally determining threshold intensity values. Two discoveries were made both of which have the potential to greatly influence the presented results. Firstly,

it was found that many materials experience two ablation regimes for higher and lower fluences respectively (28). This topic needs to be explored further, but initial research and discussions with others who posses knowledge within the laser damage field have led to the belief that the experiments presented in this thesis were done in the "higher" of the two fluence regimes. Secondly, if the first discovery is found to be true, this directly leads to the second possibility of error. The beam radius of the pulse was calculated directly from the experimental data. If this data was taken in the incorrect crater ablation regime, the calculation of the beam radius may result in a new value.

In addition to seeking answers regarding the proposed possibilities of error during experiment, alternate steps were taken in order to verify the models accuracy. The goal was to obtain literature values of the GaAs damage threshold for laser system parameters as similar to those presented in this thesis as possible. Huang *et al* and Kim *et al* both report single-shot GaAs damage fluence thresholds of 1 kJ/m^2 for 1.9 eV (635 nm) light at a pulse duration of 70 fs (29) (30). This damage fluence corresponds to a peak laser intensity of **1.34205e12** [W/cm^2]. All laser parameters were input into the model and the electron density, N_D, was given to be **4.843e21** [electrons/cm^3]. Fig 4.4 shows the simulation results. Fortunately, this value is far closer to the expected critical electron density confirming that this model is indeed promising. However, in order to increase confidence in the power and accuracy of the model, additional sets of laser parameters as well as sample materials must be tested. This puts a large emphasis on resolving experimental errors.

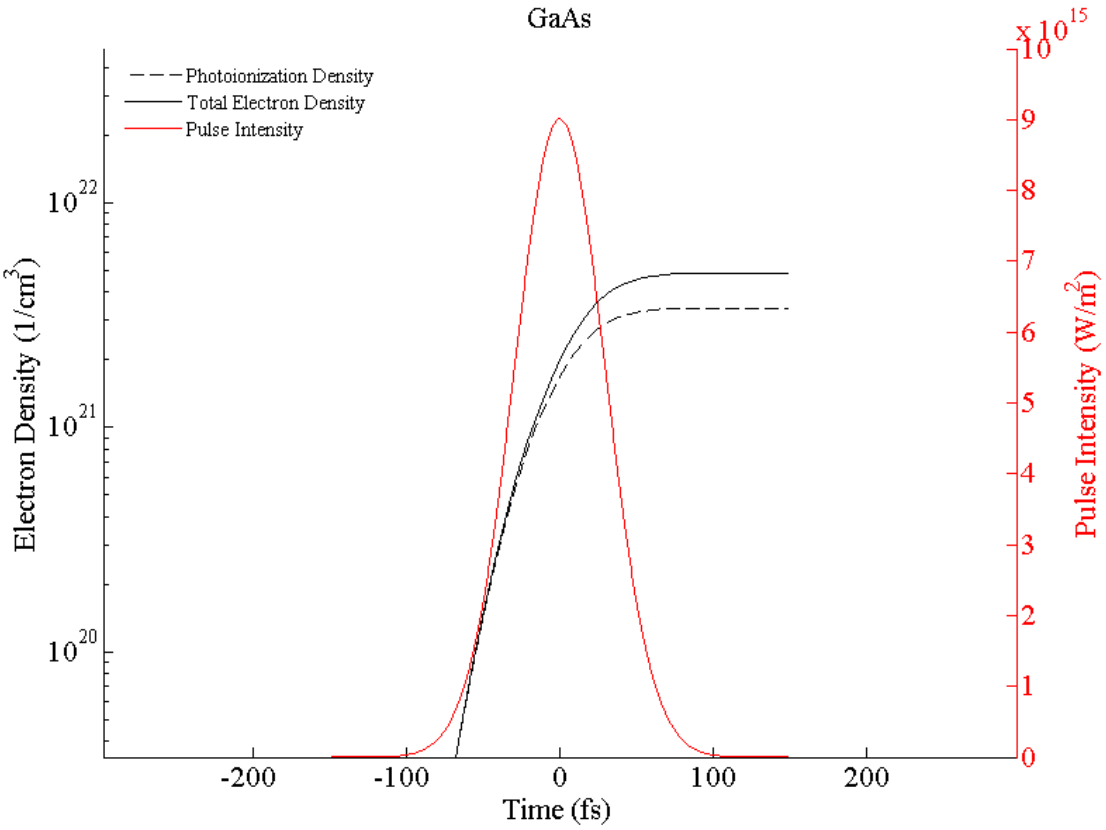

Figure 4.4: Model simulation of GaAs (band-gap 1.42eV) irradiated by 635 nm light for 70 fs at an intensity of 1.342×10^{12} Wcm^{-2}. This results in a total electron density of N_D = 4.843e21 [electrons/cm^3].

Chapter 5

Conclusion and Scope for Future Work

This thesis has discussed the background and theory behind damage mechanisms and absorption phenomena in the femtosecond laser regime. Using this theory, and ultimately Keldysh's evolution of this theory into electron density rate equations, a model was developed to predict electron density growth in optical materials under exposure to femtosecond pulses. The accuracy of this model was tested versus experimental threshold data of GaAs. Error in experimental procedures was determined to be the cause of initial discrepancies between the model predictions and the experimentally obtained data. Use of literature damage threshold values resulted in far better results. The conclusion taken from these results is that this model shows great potential, but more work must be done to increase confidence.

There are many possible routes to take in advancing the work presented in this thesis. This involves both improving the accuracy of this model, as well as adding additional capabilities. In this chapter, some of these future work topics have been discussed.

5.1 Acquire Additional Experimental Data

The most obvious way of improving the model is to compare the theoretical and experimental results for additional materials and laser parameter scenarios. This first involves correcting experimental procedures so that accurate damage thresholds can be acquired. So far, only the damage behavior of GaAs under one set of laser parameters has been tested versus model predictions. Results were very promising, but until a wider range of experimental data is obtained, the power of the model remains uncertain. If experimental damage thresholds can be resolved theoretically for a range of laser intensities, pulse durations, and wavelengths, confidence can be greatly increased. The resulting data will also allow for fitting of material properties and may lead to the addition of new capabilities.

5.2 Evolve Model to include Relaxation Mechanisms

Another way to improve the accuracy of electron density growth predictions is by understanding and modeling the recombination and relaxation mechanisms present during the experimental procedure. As of now, the model does include an "effective relaxation" term that may be used, a method described in Mero *et al* (12). However, understanding the exact mechanisms that compose this term, and modeling them separately, would lead to more accurate results. For example, another paper by Mero *et al* discusses the modeling of self-trapped excitons (STEs) to explain the physical effects behind lowered damage thresholds of dielectric films exposed to multiple femtosecond pulses (9). Here, he incorporates trap states into his full rate equation to account for STE effects.

5.3 Carrier Induced Change in Reflectivity

A feature of the model currently being developed involves taking advantage of known effects that induced carriers have on the reflectivity of a sample material. By taking the predicted electron density from the model, and accounting for any relaxation, the induced change in material reflectivity can be calculated. Through comparing the predicted reflectivity change to experimental pump-probe response signals, another means to improve model accuracy is established. Also, this method can lead to an evolution of the model to predict the composition of an unknown optical system using experimental pump-probe response data as input.

Appendix A

Theoretical Model of Absorption Phenomena in Optical Materials: Matlab Source Code

A.1 Main Script: Electron Density Growth

```
1 % Script to calculate the electron density growth as a function of...
      laser and material inputs.  Total electron density and ...
     photoionization only electron densities are calculated and ...
     plotted.
2 %
3 % Authors: Troy Anderson, Chris Ferris
4 % Last modified on: 4/14/2014
5
6 %% Clear Variable Space
7     clear all
```

```
8       % clc
9
10  %% Laser Properties
11  % Laser Wavelength [um]
12      lambda = .635;
13  % Radial Frequency [rad/s]
14      omega = 2*pi*3e8/(lambda * 10^(-6));
15  % Pulse Duration (FWHM) [fs]
16      T_FWHM = 70;
17  % Time at which irradiance is 1/e^2 of peak Intensity
18      tau = T_FWHM/1.177;
19  % Peak Laser Intensity [W/cm^2] later adjusted by transmission ...
        percent and converted to [W/m^2]
20      I_unadjusted = 1.342e12;
21
22  %% Calculate Peak Laser Intensity by providing beam power, radius ...
        and rep rate.
23  % % Laser Power [mW]
24      % P = 0;
25      % P2 = P.*(1e-3); % Convert to [W]
26  % % Beam Radius [m]
27      % w_0 = 0;
28  % % Pulse Repetition Rate, pulses per second
29      % RepRate = 1000;
30      % Ep = P2./RepRate; % beam energy calculation
31  % % Calculation of Peak Intensity [W/cm^2]
32  % Later adjusted by transmission percent and converted to units [W...
        /m^2]
33      % I_unadjusted2 = (4.*Ep)./((w_0^2).*(pi^(3/2)).*(tau*(10^-15)...
            ).*(sqrt(2)));
34
```

```
35 %% Material Properties
36 % Select material using parameter matFlag.
37 % Values for matFlag:
38 % 1: Fused Silica (Δ = 9 eV)
39 % 2: Fused Silica (Δ = 7.5 eV)
40 % 3: GaAs
41 % 4: ZnSe
42 % 5: Ge
43 % 6: HfO2
44 % 7: TiO2
45 % 8: Ta2O5
46 % 9: Al2O3
47 % 10: SiO2
48     matFlag = 3;
49 % Electron Rest Mass [kg]
50     me0 = 9.11e-31;
51 % Electron Charge [C]
52     e = 1.6e-19;
53 % Function that returns material refractive index, nonlinear ...
       refractive index, bandgap, effective mass, avalanche ...
       coefficient, effective recombination time, and reflectivity.
54     [n0, n2, Δ, me, alpha, T_recombination, T] = material_flag(...
           matFlag, lambda, me0, e);
55
56 %% Peak Intensity Adjustments and Conversion/Complex Refractive ...
       Index Calculation
57 % Peak intensity adjusted by transmission
58     I_0 = I_unadjusted.*T;
59     % I_02 = I_unadjusted2.*T;
60 % Convert peak intensity to [W/m^2]
61     I = I_0/(1e-4);
```

```
62      % I = I_02/(1e-4);
63  % Calculate refractive index using nonlinear term
64      n = n0 + n2.* I;
65
66  %% Calculate Electron Density
67  % If desired, the program allows for an array input of intensity.
68
69  % Define timescale over which the pulse is defined [fs]
70  % Value of tau*5 chosen as max to assure the tails of the gaussian...
        approach 0
71      t_span = [0, tau*5];
72  % Offset gaussian distribution to be in the center of t_span
73      offset = (t_span(2)-t_span(1))/2; % [fs]
74  % Initialize time and electron density variables
75      T = cell(1,length(I)); % [fs]
76      T2 = T;
77      Ne = cell(1,1); % [electrons/cm^3]
78      Ne2 = Ne;
79  % Variable to track final density values for each cell when I is ...
       an array.
80      FinalDensity = zeros(1,length(I));
81
82  % Calculate electron density for all intensity values
83   for i = 1:length(I)
84      % Create anonymous function to describe the intensity as a ...
           function of time. The total expression for a Gaussian laser...
            pulse is:
85      %       I(t,r) = I_0 exp(-2t^2/tau^2) exp(-2r^2/w_0^2)
86      % Where:
87      %   I_0 = 4 E_p w_0^(-2) tau^(-1) pi^(-3/2) 2^(-1/2)
88      %       E_p: pulse energy
```

```
89      %       tau: e^(-2) intensity pulse duration
90      %       w_0: beam radius
91        It = @(t) I(i).*exp(-2*(t-offset).^2./tau^2); % On-axis (r...
              =0) intensity [W/m^2]
92
93      % This function calculates the full and photoexcitation rate ...
            with time [fs] and Ne as the only inputs.  This is ...
            necessary for use with ode45 (or other ODE solvers).  ...
            Because it is an anonymous function, any function calls ...
            here have access to all variables in the workspace.
94      % Inputs:
95      %   - t: time [fs]
96      %   - Ne: Free electron density [electrons/cm^3]
97      % Outputs:
98      %   - Photoexcitation Rate and Full Rate [electrons/fs/cm^3]
99
100     % Full rate equation with and without recombination term
101         fullRate = @(t,Ne) (alpha * It(t) * Ne).*10^-19 + ...
                keldysh_full(omega,me,Δ,n(i),It(t)).*10^(-15)./100^3;
102         % fullRate = @(t,Ne) (alpha * It(t) * Ne).*10^-19 + ...
                keldysh_full(omega,me,Δ,n(i),It(t)).*10^(-15)./100^3 - ...
                Ne./T_recombination;
103
104     % Photoionization rate equation [electrons/fs/cm^3]
105         photoexcitationRate = @(t2,Ne2)keldysh_full(omega,me,Δ,n(i...
                ),It(t2)).*10^(-15)./100^3;
106
107     % Solve the differential equation to get the density of ...
            electrons. Note that since the rate equations are defined ...
            as anonymous functions, the @ symbol is not needed in the ...
            ode45 call.  [fs, electrons/cm^3]
```

```
108      [T{i},Ne{i}] = ode45(fullRate,t_span,0);
109      [T2{i},Ne2{i}] = ode45(photoexcitationRate,t_span,0);
110
111      FinalDensity(i) = Ne{i}(end);
112   end
113
114 %% Find the total electron densities.  Used to adjust plot limits.
115 % choose desired cell
116      get_array = Ne{1,1};
117      get_array2 = Ne2{1,1};
118 % get final density for total and photoionization only electron ...
       densitites
119      density = get_array(end);
120      density2 = get_array2(end);
121
122 %% Plotting the Evolution of Electron Density
123 % The laser pulse, total electron density, and photionization ...
       density are graphed within the same figure.
124
125 % Development of the figure
126      t = linspace(t_span(1),t_span(2),1000);
127      [AX,H1,H2] = plotyy(T2{1}-offset,Ne2{1},t-offset,It(t),'...
           semilogy','plot');
128      set(AX,'xlim',[-t_span(2) t_span(2)]);
129      hold all
130      AX2 = semilogy(T{1}-offset,Ne{1},'k');
131      ylim([density2/100 density*10])
132 % Labels, legend, and plot styles are adjusted
133      xlabel('Time (fs)');
134      set(H1,'LineStyle','--','color','k')
135      set(H2,'color','r')
```

```
136      set(AX(1),'ycolor','k')
137      ylabel(AX(1),'Electron Density (1/cm^3)')
138      set(AX(2),'ycolor','r')
139      ylabel(AX(2),'Pulse Intensity (W/m^2)')
140      [legh, objh] = legend([AX2 H1 H2],'Total Electron Density', '...
             Photoionization Density', 'Pulse Intensity');
141      set(legend('Location','NorthWest'));
142      set(legend,'FontSize',10)
143      legend boxoff
144      title('GaAs');
145
146  % display final density value
147      disp('Density');
148      disp(density);
149
150  % Save image as material.png within path folder
151  % print('-dpng', '-r300', material)
```

A.2 Script: Material_Flag

```
1  % This script utilizes a case structure and input variable '...
       matFlag' for material selection.  The additional inputs are ...
       necessary for calculations of other material paramaters.  ...
       Returned to the main script are material refractive index, ...
       nonlinear refractive index, bandgap, effective mass, avalanche ...
       coefficient, effective recombination time, and transmission ...
       value.
```

```
2  % Of note, material values have been taken from literature, fit ...
       using experimental results, or left blank until experimental ...
       results can be obtained.  The Sellmeier Equation, refractive ...
       index values, and reflectivity values can be found at http://...
       refractiveindex.info/.
3
4  % Authors: Chris Ferris, Troy Anderson
5  % Last modified on: 4/14/2014
6
7  function [n0, n2, Δ, me, alpha, T, Trans] = material_flag(matFlag,...
       lambda, me0, e)
8  % Use a switch/case structure to select between different ...
       materials
9  % Values for matFlag:
10 % 1: Fused Silica (Δ = 9 eV)
11 % 2: Fused Silica (Δ = 7.5 eV)
12 % 3: GaAs
13 % 4: ZnSe
14 % 5: Ge
15 % 6: HfO2
16 % 7: Ti02
17 % 8: Ta2O5
18 % 9: Al2O3
19 % 10: Si02
20
21 switch matFlag
22     % Fused Silica (Replicating Gulley)
23     case 1
24         alpha = 15;              % Avalanche Coefficient (cm^2/J);
25         Δ_eV = 9;            % Bandgap [eV]
26         Δ = Δ_eV * e;    % Convert bandgap to Joules
```

```
27          me = .5 * me0;          % Effective Electron Mass [kg]
28          n0 = sqrt( 1 + 0.6961663*lambda^2/(lambda^2-0.0684043^2) +...
                ...
29              0.4079426*lambda^2/(lambda^2-0.1162414^2) + ...
30              0.8974794*lambda^2/(lambda^2-9.896161^2) );
31          n2 = 2.48e-16;          % Nonlinear refractive index [cm...
                ^2/W]
32          T = 2000;               % Effective recombinatino time [fs...
                ]
33          Ref = 0.03414;          % Reflectivity (800nm) must adjust...
                for other incident wavelengths
34          Trans = 1 - Ref;
35
36      % Fused Silica (replicating Schaffer).  Note: Schaffer's ...
            calculation of the electric field (F) uses 'I' rather than ...
            '2*I' in the numerator.  This is incorrect.  Removing the ...
            '2' from the equation below will reproduce the graphs in ...
            his paper.
37      case 2
38          alpha = 1.6;
39          Δ_eV = 7.5;
40          Δ = Δ_eV * e;
41          me = .5 * me0;
42          n0 = sqrt( 1 + 0.6961663*lambda^2/(lambda^2-0.0684043^2) +...
                ...
43              0.4079426*lambda^2/(lambda^2-0.1162414^2) + ...
44              0.8974794*lambda^2/(lambda^2-9.896161^2) );
45          n2 = 0;
46          T = 2000;
47          Ref = 0.03414;          % 800nm
48          Trans = 1 - Ref;
```

```
49
50      % GaAs
51      case 3
52          alpha = 10;
53          Δ_eV = 1.424;
54          Δ = Δ_eV * e;
55          me = 0.067 * me0;
56          format long, n0 = sqrt( 3.5 + 7.4969*lambda^2/(lambda^2-0...
                .4082^2) + ...
57              1.9347*lambda^2/(lambda^2-37.17^2) );
58          n2 = 0;
59          T = 0;
60          Ref = 0.32852;          % 800nm
61          Trans = 1 - Ref;
62
63      % ZnSe
64      case 4
65          alpha = 5;
66          Δ_eV = 2.70;
67          Δ = Δ_eV * e;
68          me = 0.17 * me0;
69          n0 = sqrt(1 + 4.298*lambda^2/(lambda^2-0.1921^2) + ...
70              0.6278*lambda^2/(lambda^2-0.3788^2) + ...
71              2.896*lambda^2/(lambda^2-46.995));
72          n2 = 0;
73          T = 0;
74          Ref = 0.18699;          % 800nm
75          Trans = 1 - Ref;
76      % Ge
77      case 5
78          alpha = 0;
```

```
79          Δ_eV = 0.66;
80          Δ = Δ_eV * e;
81          me = 0.041 * me0;
82          if lambda == .8
83              n0 = 4.7;
84          elseif lambda == 1.5
85              n0 = 4.2796;
86          else
87              n0 = 4.35;          % use http://refractiveindex.info...
                    /;
88          end
89          n2 = 0;
90          T = 0;
91          Ref = 0.42246;          % 800nm
92          Trans = 1 - Ref;
93
94      % Hf02
95      case 6
96          alpha = 10;
97          Δ_eV = 5.1;
98          Δ = Δ_eV * e;
99          me = 0.45 * me0;
100         n0 = 1.8946;            % use http://refractiveindex.info...
                /;
101         n2 = 0;
102         T = 1050;
103         Ref = 0.09552;          % 800nm
104         Trans = 1 - Ref;
105
106     % TiO2
107     case 7
```

```
108         alpha = 34;
109         Δ_eV = 3.30;
110         Δ = Δ_eV * e;
111         me = 1.26 * me0;
112         n0 = sqrt( 5.913 + 0.2441*lambda^2/(lambda^2-0.0803^2));
113         n2 = 0;
114         T = 120;
115         Ref = 0.18643;          % 800nm
116         Trans = 1 - Ref;
117
118     % Ta2O5
119     case 8
120         alpha = 11;
121         Δ_eV = 3.5;
122         Δ = Δ_eV * e;
123         me = 0.100 * me0;
124         if lambda == .8
125             n0 = 1.80;
126         elseif lambda == 1.5
127             n0 = 1.78;
128         else
129             n0 = 1.85;          % use http://refractiveindex.info...
                    /;
130         end
131         n2 = 0;
132         T = 490;
133         Ref = 0.07940;          % 800nm
134         Trans = 1 - Ref;
135
136     % Al2O3
137     case 9
```

```
138         alpha = 12;
139         Δ_eV = 6.5;
140         Δ = Δ_eV * e;
141         me = 0.35 * me0;
142         n0 = sqrt( 1 + 1.4313*lambda^2/(lambda^2-0.07266^2) + ...
143             0.6505*lambda^2/(lambda^2-0.1193^2) + 5.3414*lambda...
                    ^2/(lambda^2-18.028));
144         n2 = 0;
145         T = 220;
146         Ref = 0.0758;           % 800nm
147         Trans = 1 - Ref;
148
149     % Si02
150     case 10
151         alpha = 8;
152         Δ_eV = 8.3;
153         Δ = Δ_eV * e;
154         me = 0.75 * me0;
155         n0 = sqrt( 1 + 0.6657*lambda^2/(lambda^2-0.060^2) + ...
156             0.5035*lambda^2/(lambda^2-0.106^2) + 0.2148*lambda^2/(...
                    lambda^2-.119^2) + ...
157             0.5392*lambda^2/(lambda^2-8.792^2) + 1.808*lambda^2/(...
                    lambda^2-19.70^2));
158         n2 = 0;
159         T = 220;
160         Ref = 0.04498;           % 800nm
161         Trans = 1 - Ref;
162
163     otherwise
164         disp('Warning: Invalid material parameters');
165        return
```

```
166
167 end
168 end
```

A.3 Script: Keldysh Rates Versus Keldysh Parameter

```
1 % Program to calculate the photoexcitation rate as a function of ...
    intensity as described in Keldysh (L. Keldysh, "Ionization in ...
    the field of a strong electromagnetic wave," Soviet Physics ...
    JETP 20, 1307–1314 (1965).
2 %
3 %  The program separately calculates the expressions for ...
    multiphoton excitation, tunneling, and the full Keldysh ...
    expression.
4
5 % Authors: Chris Ferris, Troy Anderson
6 % Last modified on: 4/14/2014
7
8 clear all
9
10 %% Constants:
11 % Speed of light (m/s)
12     c = 3e8;
13 % Electron Charge (C)
14     e = 1.6e-19;
15 % Electron Rest Mass (kg)
```

```
16      me0 = 9.11e-31;
17
18  %% Laser and Material Parameters
19  % Wavelength (um)
20      lambda = 0.8;
21  % Radial Frequency (rad/s)
22      w = 2*pi()*c/(lambda * 10^(-6));
23  % Select material using parameter matFlag.
24  % Values for matFlag:
25  % 1: Fused Silica (Δ = 9 eV)
26  % 2: Fused Silica (Δ = 7.5 eV)
27  % 3: GaAs
28  % 4: ZnSe
29  % 5: Ge
30  % 6: HfO2
31  % 7: Ti02
32  % 8: Ta2O5
33  % 9: Al2O3
34  % 10: Si02
35      matFlag = 1;
36  % Function that returns material refractive index, nonlinear ...
        refractive index, bandgap, effective mass, avalanche ...
        coefficient, effective recombination time, and reflectivity.
37      [n0, n2, Δ, me, alpha, T_recombination, T] = material_flag(...
            matFlag, lambda, me0, e);
38
39  %% Range of Laser Intensities
40      Icm_min = 12; % Order of magnitude of minimum laser [W/cm^2] (...
            a value of X corresponds to 10^X W/cm^3)
41      Icm_max = 15; % Order of magnitude of maximum laser [W/cm^2]
42      Icm = logspace(Icm_min,Icm_max,50); % [W/cm^2]
```

```
43
44      I = Icm.*100^2; % Convert to [W/m^2]
45
46      n = n0 + n2 .* Icm;       % Calculate refractive index using ...
            nonlinear term
47
48  %% Calculation of Keldysh Parameter (Keldysh p 1312 between eqns ...
        36 & 37)
49  gamma = keldysh_param(w,me,Δ,n,I);       %unitless
50
51  %% Calculations of Keldysh Tunneling Rate (Keldysh eq 40)
52  Wtun = keldysh_tunneling(w,me,Δ,n,I);    % [electrons/s/m^3]
53  Wtun_scaled = Wtun *10^(-15) / 100^3;        % [electrons/fs/cm^3]
54
55  %% Calculation of Keldysh MPI Rate (Keldysh eq 41)
56  Wmpi = keldysh_MPI(w,me,Δ,n,I);          % [electrons/s/m^3]
57  Wmpi_scaled = Wmpi *10^(-15)  / 100^3;       % [electrons/fs/cm^3]
58
59  %% Calculation of Full Keldysh Expression (Keldysh eq 37)
60  Wfull = keldysh_full(w,me,Δ,n,I);        % [electrons/s/m^3]
61  Wfull_scaled = Wfull *10^(-15) / 100^3;      % [electrons/fs/cm^3]
62
63  %% Plot Data
64  material = 'Material';       % Plot Title
65  % Plot Tunneling, MPI, and Full Rates Versus Intensity
66  figure
67  subplot(2,1,1)
68  loglog(Icm,Wtun_scaled,'--', Icm,Wmpi_scaled,':', Icm,Wfull_scaled...
        );
69
70  axis([10^Icm_min 10^Icm_max 1e1 1e30])
```

```
71 xlabel('Intensity (W/cm^2)');
72 ylabel('Photoionization Rate (1/fs/cm^3)');
73 plot_legend = legend('Tunneling', 'MPI','Full');
74 set(plot_legend,'FontSize',8)
75 title(material);
76 % Plot Keldysh Parameter Vs Intensity
77 subplot(2,1,2)
78 loglog(Icm,gamma);
79 xlabel('Intensity (W/cm^2)');
80 ylabel('Keldysh Parameter (\gamma)');
81 % Save Figure as a .png file with filename material
82 print('-dpng', '-r300', material)
```

A.4 Script: Full Keldysh Rate

```
1  function W = keldysh_full(w,me,Δ,n,I)
2  % Function to calculate the full Keldysh rate (eq 37 from Keldysh ...
       (1965))
3  %
4  % Inputs:
5  %   - w: radial frequency of light (omega) [rad/s]
6  %   - me: effective electron mass [kg]
7  %   - Δ: bandgap of material [J]
8  %   - n: refractive index [unitless]
9  %   - I: Laser Irradiance [W/m^2]
10 % Outputs:
11 %   - W: Keldysh photoionization rate [electrons/s/m^3]
12 %
```

```
13 % Note: There are two ways to calculate the dawson integral within...
       this function.  One is through mfun, which is supplied with ...
      the symbolic math toolbox.  The other is through dawson.m, ...
      which is a file from Matlab File Exchange that is faster.
14 %
15 % Authors: Troy Anderson, Chris Ferris
16 % Last modified on 4/14/2014
17
18 %% Constants:
19 % Speed of light [m/s]
20     c = 3e8;
21 % Electron Charge [C]
22     e = 1.6e-19;
23 % Permittivity of Free Space [F/m]
24     ep0 = 8.85e-12;
25 % Planck Constant [J s]
26     hbar = 1.054*10^(-34);
27
28 %% Calculations
29 % Electric Field Strength
30     F = sqrt((2*I)./(c*n*ep0)); %[V/m]
31 % Gamma, Keldysh Parameter
32     gamma = (w./(e.*F)).*sqrt(me*Δ); % [unitless]
33 % Create variables for common terms
34     gg = gamma.^2./(1+gamma.^2);
35     g1 = 1./(1+gamma.^2);
36
37 % Elliptic Integrals
38 % Elliptic Integrals: Keldysh expressions assume modulus k (m = k...
      ^2).  Since ellipke uses modulus m, the expressions for gg and ...
      g1 are squared relative to those found in Keldysh
```

```
39      [Kg,Eg] = ellipke(gg);
40      [K1,E1] = ellipke(g1);
41
42      Δ_tau = 2*Δ*sqrt(1+gamma.^2).*E1./(pi()*gamma);
43      X = floor(Δ_tau./(hbar*w)+1);
44
45      Wf1 = 2*w/(9*pi()) .* (sqrt(1+gamma.^2) * me * w ./ (gamma * ...
            hbar)).^(3/2);
46      Wf2 = Qfun(gamma,Δ_tau./(hbar*w));
47      Wf3 = exp(-pi().*X.*(Kg-Eg)./E1);
48
49      W = Wf1 .* Wf2 .* Wf3;  % [electrons/s/m^3]
50
51  % Set all NaN values to 0.  NaNs can occur if the value of the ...
        intensity is too small.  In this case, the photoionization rate...
         is negligible.
52      W(isnan(W)) = 0;
53
54  %% Nested Subfunctions
55  % Q function (from Keldysh)
56
57      function Q = Qfun(gamma,x)
58          Q1 = sqrt(pi()./(2.*K1));
59          Q2 = zeros(1,length(gamma));
60
61          for i = 1:length(gamma)
62              j = 0;
63              tol = 1e-3;
64              err = 1;
65              OldQ2 = 0;
66              while err > tol
```

```
67
68                  % Check to see if user-supplied 'dawson.m' exists ...
                        in the path.  This function is a faster ...
                        implementation of the dawson integral than the ...
                        'mfun' implementation.
69                  if exist('dawson.m','file') == 2
70                      Q2(i) = Q2(i) + exp(-pi() .* (Kg(i)-Eg(i)) .* ...
                            j ./ E1(i)) .* dawson(sqrt(pi()^2.*(2*floor...
                            (x(i)+1)-2.*x(i) + j) ./(2*K1(i) .* E1(i)))...
                            );
71                  else
72                      Q2(i) = Q2(i) + exp(-pi() .* (Kg(i)-Eg(i)) .* ...
                            j ./ E1(i)) .* mfun('dawson',sqrt(pi()^2....
                            *(2*floor(x(i)+1)-2.*x(i) + j) ./(2*K1(i) ....
                            * E1(i))));
73                  end
74                  err = abs(Q2(i) - OldQ2);
75                  j = j + 1;
76                  OldQ2 = Q2(i);
77              end
78          end
79          Q = Q1.*Q2;
80      end
81  end
```

A.5 Script: Keldysh Tunneling Rate

```
1  function [W] = keldysh_tunneling(w,me,Δ,n,I)
```

```
2  % Function to calculate the Keldysh tunneling rate (eq 40 from ...
       Keldysh (1965))
3  %
4  % Inputs:
5  %   - w: radial frequency of light (omega) [rad/s]
6  %   - me: effective electron mass [kg]
7  %   - Δ: bandgap of material [J]
8  %   - n: refractive index [unitless]
9  %   - I: Laser Irradiance [W/m^2]
10 % Outputs:
11 %   - W: Keldysh Tunneling Rate [electrons/s/m^3]
12 %
13 % Authors: Chris Ferris, Troy Anderson
14 % Last modified on 4/14/2014
15
16 %% Constants:
17 % Speed of light [m/s]
18     c = 3e8;
19 % Electron Charge [C]
20     e = 1.6e-19;
21 % Permittivity of Free Space [F/m]
22     ep0 = 8.85e-12;
23 % Planck Constant [J.s]
24     hbar = 1.054*10^(-34);
25
26 %% Calculations
27 % Electric Field Strength [V/m]
28     F = sqrt((2*I)./(c*n*ep0));
29
30     Wtun1 = (2*Δ)/(9*hbar*pi()^2) * ((me*Δ)/hbar^2)^(3/2);
31     Wtun2 =  ((e*hbar*F)./(me^(1/2)*Δ^(3/2))).^(5/2);
```

```
32
33      Wtun3 = exp(-(pi()*me^(1/2)*Δ^(3/2))./(2*e*hbar*F) .* (1-(me*w...
            ^2*Δ)./(8*e^2*F.^2)));
34
35      W = Wtun1 .* Wtun2 .*Wtun3;      % [electrons/s/m^3]
36
37  end
```

A.6 Script: Keldysh MPI Rate

```
1   function [W] = keldysh_MPI(w,me,Δ,n,I)
2   % Function to calculate the Keldysh tunneling rate (eq 41 from ...
        Keldysh (1965))
3   %
4   % Inputs:
5   %   - w: radial frequency of light (omega) [rad/s]
6   %   - me: effective electron mass [kg]
7   %   - Δ: bandgap of material [J]
8   %   - n: refractive index [unitless]
9   %   - I: Laser Irradiance [W/m^2]
10  % Outputs:
11  %   - W: Keldysh MPI Rate [electrons/s/m^3]
12  %
13  % Note: There are two ways to calculate the dawson integral within...
        this function.  One is through mfun, which is supplied with ...
       the symbolic math toolbox.  The other is through dawson.m, ...
       which is a file from Matlab File Exchange that is faster.
14  %
```

```
15 % Authors: Chris Ferris, Troy Anderson
16 % Last modified on 4/14/2014
17
18 %% Constants:
19 % Electron Charge [C]
20     e = 1.6e-19;
21 % Planck Constant [J s]
22     hbar = 1.054e-34;
23 % Speed of light (m/s)
24     c = 3e8;
25 % Permittivity of Free Space (F/m)
26     ep0 = 8.85e-12;
27
28 %% Calculations
29 % Electric Field Strength [V/m]
30     F = sqrt((2*I)./(c*n*ep0));
31
32     Δ_tau = Δ + (e^2.*F.^2)./(4*me*w^2);
33
34     X = fix(Δ_tau./(hbar.*w) +1);
35
36     Wmpi1 = (2*w)/(9*pi()) * ((me*w)/hbar)^(3/2);
37
38 % Check to see if user-supplied 'dawson.m' exists in the path.  ...
      This function is a faster implementation of the dawson integral...
       than the 'mfun' implementation.
39 if exist('dawson.m','file') == 2
40     Wmpi2 = dawson(((2.*X-(2.*Δ_tau)./(hbar*w)).^(1/2)));
41 else
42     Wmpi2 = mfun('dawson',((2.*X-(2.*Δ_tau)./(hbar*w)).^(1/2)));
43 end
```

```
44
45      Wmpi3 = exp(2.*X.*(1-(e^2.*F.^2)./(4*me*w^2*Δ)));
46      Wmpi4 = ((e^2.*F.^2)./(16*me*w^2*Δ)).^X;
47
48  W = Wmpi1 .* Wmpi2 .* Wmpi3 .* Wmpi4;    % [electrons/s/m^3]
49  end
```

Bibliography

[1] C. B. Schaffer, A. Brodeur, and E. Mazur, Measurement Science and Technology **12**, 1784 (2001).

[2] S. C. Jones, P. Braunlich, R. T. Casper, and X.-A. Shen, Optical Engineering **28**, 1039 (1989).

[3] L. V. Keldysh, Soviet Physics Jetp **20**, 1307 (1965).

[4] B. C. Stuart, M. D. Feit, S. Herman, A. M. Rubenchik, B. W. Shore, and M. D. Perry, Physical Review B **53**, 1749 (1996).

[5] R. Wood, *Laser Damage in Optical Materials*, Optics and Optoelectronics Series (A. Hilger, 1986) ISBN 9780852747926.

[6] M. J. Soileau, W. E. Williams, E. W. V. Stryland, T. f. Boggess, and A. L. Smirl, Natl Bur. Stand **669**, 387 (1984).

[7] B. C. Stuart, M. D. Feit, S. Herman, A. Rubenchik, B. W. Shore, and M. D. Perry, J. Opt. Soc. Am. B **13**, 459 (1996).

[8] H. Sun, T. Jia, C. Li, X. Li, S. Xu, and D. Feng, Solid State Communications **141**, 127 (2007).

[9] M. Mero, B. Clapp, J. C. Jasapara, and W. Rudolph, Optical Engineering **44**, 1 (2005).

[10] R. T. Williams, Optical Engineering **28**, 1024 (1989).

[11] A. Hertwig, S. Martin, J. Kruger, and W. Kautek, Applied Physics A **79**, 1075 (2004).

[12] M. Mero, J. Liu, W. Rudolph, D. Ristau, and K. Starke, Physical Review B **71**, 1 (2005).

[13] A. von Hippel, Z. Phys. **75**, 145 (1932).

[14] E. Yablonovitch and N. Bloembergen, Physical Review Letters **29**, 907 (1972).

[15] D. Du, X. Liu, G. Korn, and J. Squier, Applied Physics Letters **64**, 3071 (1994).

[16] Coherent Laser Group, 5100 Patrick Henry Drive, Santa Clara, CA, *Multiphoton Excitation Microscopy: MPE Tutorial* (2000).

[17] S. H. Lin, A. A. Villaeys, and Y. Fujimura, *Advances in Multi-Photon Processes and Spectroscopy* (World Scientific, 2011).

[18] M. N. Polyanskiy, "Refractive index database," http://refractiveindex.info.

[19] T. Anderson, "Gaussian beams: Important calculations," (2013).

[20] C. B. Schaffer, *Interaction of Femtosecond Laser Pulses with Transparent Materials*, Ph.D. thesis, Harvard University (2001).

[21] P. J. Acklam, "dawson.m," Matlab File Exchange (2004).

[22] J. R. Gulley, Optical Engineering **51**, 1 (2012).

[23] A. Vaidyanathan, T. W. Walker, A. H. Guenther, S. S. Mitra, and L. M. Narducci, Physical Review B **20**, 19 (1979).

[24] L. M. Narducci, Physical Review B **14**, 2508 (1976).

[25] J. M. Liu, Optics Letters **7**, 196 (1982).

[26] J. Bonse, J. M. Wrobel, J. Kruger, and W. Kautek, Applied Physics A **72**, 89 (2001).

[27] N. Semaltianos, W. Perrie, P. french, M. Sharp, G. Dearden, S. Logothetidis, and K. Watkins, Applied Physics A **94**, 999 (2009).

[28] D. J. hwang, C. P. Grigoropoulos, and T. Y. Choi, Journal of Applied Physics **99**, 1 (2006).

[29] L. Huang, J. P. Callan, E. N. Glezer, and E. Mazur, Physical Review Letters **80**, 185 (1997).

[30] A. M. T. Kim, J. Callan, C. Roeser, and E. Mazur, Physical Review B **66**, 1 (2002).